International
Progress Report

IPR-04-42

Äspö Hard Rock Laboratory

Äspö Task Force

Task 6A, 6B and 6B2

Simulation of tracer transport considering both experimental and natural time scales

Urban Svensson
Computer-aided Fluid Engineering AB

Sven Follin
SF GeoLogic AB

August 2004

Svensk Kärnbränslehantering AB
Swedish Nuclear Fuel
and Waste Management Co
Box 5864
SE-102 40 Stockholm Sweden
Tel 08-459 84 00
+46 8 459 84 00
Fax 08-661 57 19
+46 8 661 57 19

Äspö Hard Rock
Laboratory

Report no.
IPR-04-42

No.
F65K

Author
Urban Svensson
Sven Follin

Date
2004-08-01

Checked by
Jan-Olof Selroos

Date
2004-11-16

Approved
Christer Svemar

Date
2004-11-17

Äspö Hard Rock Laboratory

Äspö Task Force

Task 6A, 6B and 6B2

Simulation of tracer transport considering both experimental and natural time scales

Urban Svensson
Computer-aided Fluid Engineering AB

Sven Follin
SF GeoLogic AB

August 2004

Keywords: Transport, Retention, Model, Transients, DarcyTools

Abstract

Results for Task 6A, 6B and 6B2 are reported. Simulations are carried out using the code DarcyTools. Transport simulations are based on a particle tracking method.

Comparisons with field data show that fair agreement can be achieved for weakly and non sorbing tracers, while strongly sorbing tracers are less successfully simulated. As the model used is focussed on diffusive exchange processes, the results for strongly sorbing tracers may point to a limitation in the approach adopted.

The influence of pressure transients is discussed and a simple test case is presented. It is suggested that one may need to consider the effects of transients when long term simulations are attempted.

Sammanfattning

Resultat för Task 6A, 6B och 6B2 redovisas. Beräkningarna baseras på datorprogrammet DarcyTools. Transportsimuleringarna genomförs med en partikel-följande metod.

Jämförelser med fältdata visar att acceptabel överensstämmelse kan erhållas för svagt och icke sorberande spårämnen. Starkt sorberande ämnen ger inte lika bra resultat. Beräkningsmodellen utgår ifrån att utbytesprocesser är av diffusiv natur. För starkt sorberande ämnen är eventuellt kemiska reaktioner viktigare, vilket i så fall pekar på en begränsning i det valda angreppssättet.

Effekten av transienta tryckpulser diskuteras i rapporten och ett numeriskt experiment redovisas. Resultaten antyder att transienta effekter kan vara av betydelse vid långtidstransport.

Contents

1 Introduction

1.1 Background

A general introduction to Task 6 is given by Dershowitz et al. (2003), from where we quote:

Although site characterisation codes and performance assessment codes use similar physical concepts, their constructions differ due to their different purposes. Site characterisation codes represent the entire flow system of a volume of rock. The models include full three-dimensional representations of the major conducting features, either as discrete features or stochastic continua. The boundary conditions attempt to be detailed and realistic. Site characterisation codes are used to design, predict, and analyse experimental activities. They are used to test conceptual models of the hydrostructural framework, and to develop realistic flow and transport parameters.

Site characterisation codes, because of their detail, require significant effort in their construction and execution. Site characterisation codes often require extensive and time-consuming calibration to available field data.

Performance assessment codes have different purposes than site characterisation codes. Performance assessment codes consider a wide range of scenarios for the projected post-closure life of a repository. These problems often include all relevant features, events, and processes with all their attendant uncertainties. Hence, a performance assessment code must be capable of producing many realisations by being very fast and flexible. Due to their detail and complexity, site characterisation codes are generally not practical for direct application to performance assessment problems where many parameters must be systematically varied, or many different scenarios must be tested.

Performance assessment codes respond to these requirements by simplifying the description of the flow system and abstracting the natural system to one-dimensional pathways or networks of one-dimensional pathways. These pathways and their associated properties may be extracted from the results of site characterisation codes. With these simple models, one can run many scenarios and variations over the long time scales that are required for performance assessment calculations.

The process of simplification from site characterisation data to performance assessment codes should involve an extraction of the critical aspects of the site characterisation information. The extraction requires the reduction of a detailed site characterisation model to simple features with properties and geometries that produce equivalent flow and transport behaviours. The effectiveness of the procedure for performing these extractions from site characterisation to performance assessment is a critical issue for repository development.

Äspö Task Force Task 6 consists of a set of numerical experiments that use a common set of hydrostructural models to test performance assessment codes and site characterisation codes. The comparison of the results of these simulations serves several objectives (Benabderrahmane et al., 2000):

Assessment of simplifications used in PA models.

1. Determination of how the experimental tracer and flow experiments can constrain the range of parameters used in PA models.
2. Support of the design of site characterisation programs to assure that the results have optimal value for performance assessment calculations.
3. Better understanding of site-specific flow and transport behaviour at different scales using site characterisation models.

The objectives of Task 6 are being met through an iterative process of SC model implementation, calibration to in situ experiments, PA type simulations, and sensitivity studies. In this process Task 6 will primarily focus on the 50 to 100 m block scale (Tasks 6D and 6E) which is the critical scale for geosphere retention for many repository assessment programs. However, in order to allow for a more direct comparison, initial simulations will be carried out using data from the TRUE-1 site at the 5 metre scale (Tasks 6A, 6B and 6BII). The latter three tasks have been worked upon during 2001-2002. Irrespective of scales of application the main purpose of the modelling is to assess how different conceptualisations at the two scales considered compare to each other.

Tasks 6D and 6E is preceded by Task 6C which involves construction of a semi-synthetic block scale model which integrates available information from the Äspö HRL and which will serve as a basis for the subsequent modelling phases.

1.2 Objective

The main objective of the work to be presented is to evaluate how the methods and concepts embodied in the computer code DarcyTools (Svensson et al., 2004) perform for the problem addressed.

1.3 Outline of report

First the situation considered is described, next section, then the modelling approach used is outlined. After that the simulations requested in the Task 6 specification are carried out and discussed.

As this is the first project where DarcyTools is used for tracer transport and retention studies, some basic tests are needed. Verification, sensitivity and validation studies are compiled in Appendices A, B and C, respectively.

2 The situations considered

2.1 A general outline

The two situations considered are shown in Figure 2-1. In Task 6A and 6B, to be defined, it is a radially converging flow between boreholes KXTT1R2 and KXTT3R2 (see Figure 2-1, top) that is analysed. It is expected that the tracers follow a single narrow flow channel. All boreholes shown cross a fracture called Feature A, which has been extensively studied within the TRUE-1 project (Winberg et al., 2000).

The configuration defining Task 6B2 is shown in Figure 2-1, bottom. The tracers are now injected along a line in Feature A and one can hence expect that a larger area of the fracture is involved. This problem can be treated as two-dimensional but if fractures crossing Features A are also considered the problem becomes three-dimensional.

2.2 The mm scale view

The conceptual representation of Feature A is shown in Figure 2-2 (from Winberg et al., 2000). This representation shows Feature A as a single opening, with an aperture of about 1 mm. A range of fracture minerals and fault gouge is also indicated.

A somewhat different view is shown in Figure 2-3 (Mazurek et al., 2003). This figure is based on direct observations of a master fault at Äspö, using large diameter (25 cm) boreholes. The impression from Figure 2-3 is that a network of flow channels is found also on the mm to cm scale.

It has recently been concluded, Winberg et al. (2002), that uncertainties remain regarding the anatomy of and retention processes in Feature A.

2.3 Retention processes

A tracer moving with the fastest streamline from the injection borehole to the pumped borehole gives the shortest transport time for a certain experiment. However, only an insignificant amount of the tracer will have this travel time; most of the injected tracer will be subject to a number of retention processes that delay the transport. The most important of these are:

- Diffusion into the matrix with possible sorption on inner surfaces.
- Diffusion/sorption in fine-grained fault gouge.
- Multiple pathways, giving a range of travel times. We may include Taylor dispersion in this group.
- Equilibrium surface sorption in the flow channels.
- Diffusion into zones of stagnant water.

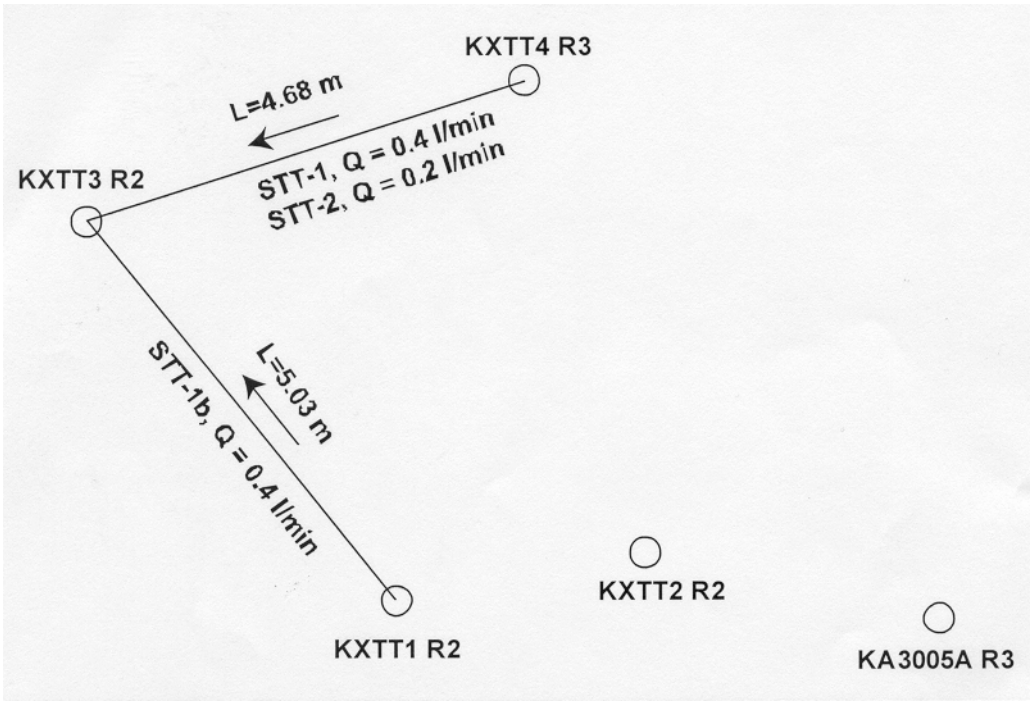

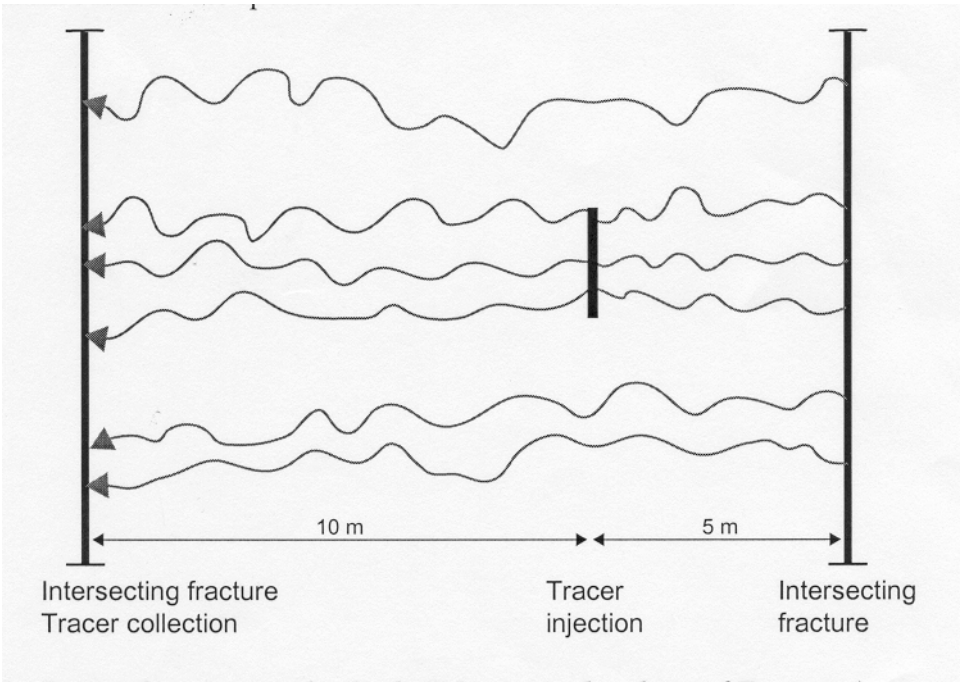

Figure 2-1. *The situation considered in Task 6A and 6B (top) and 6B2.*

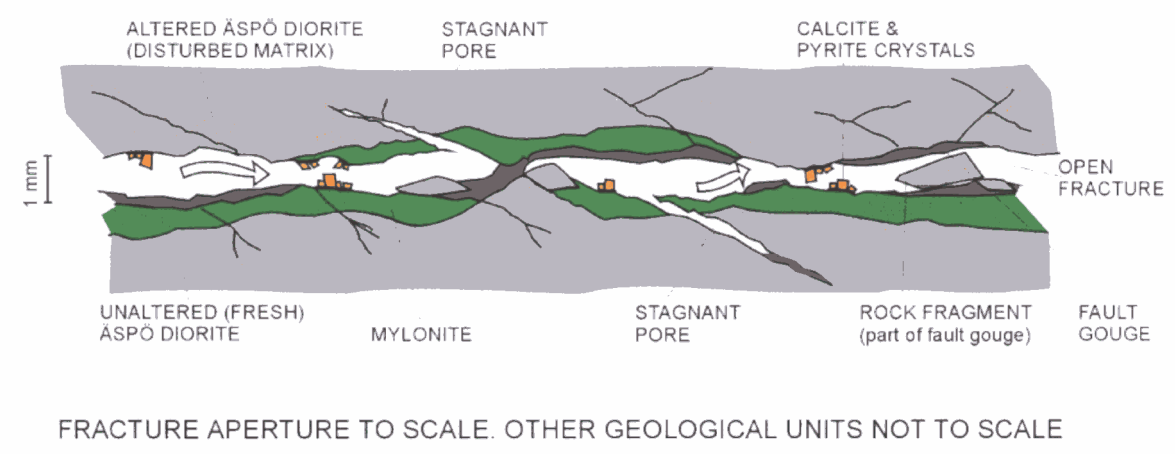

Figure 2-2. *The mm scale view. Conceptual view of Feature A as given by Winberg et al. (2000)*

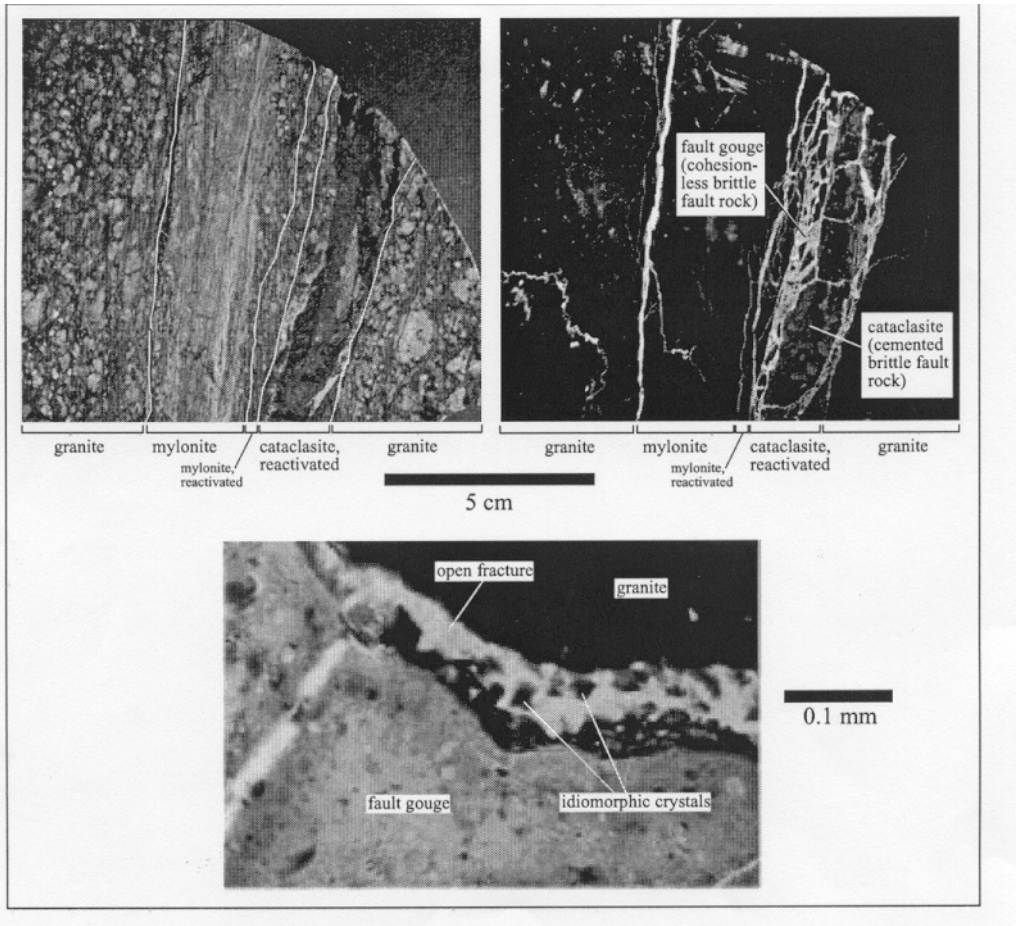

Figure 2-3. *The mm scale view. Direct observations of a master fault at Äspö (Mazurek et al., 2002).*

In the final report on the TRUE-1 experiment (Winberg et al., 2000) it is concluded that diffusion/sorption in the rock matrix is the dominating retention mechanism in Feature A. However, Mazureck et al. (2003) and Jakob et al. (2003) emphasize the role of the gouge material and Dershowitz et al. (2000) do not exclude any of the listed processes.

In a recent paper Neretnieks (2002) advocates "diffusion into the stagnant water zones in the fracture" as a key retention process. Also Dershowitz et al. (2000) argue that the effect of more stagnant water volumes may be significant (the Miller advective immobile exchange approach). The role of stagnant water in the fracture plane will be discussed also in the present report and we will therefore elaborate some thoughts and suggestions by the present authors.

The discussion will be based on Figure 2-4, where a conceptual view of flow and transport in a fracture plane is illustrated. The size of the plane is of the order 10 x 10 m^2 and the discussion will focus on "natural conditions" (the radially converging case may be quite different). The first point to note is that only one major flow channel is indicated. This is no more than a guess, as studies on the 10 cm scale (Hakami, 1995) show several parallel streamlines. On the large scale there is however evidence that "most of the water is carried in relatively few flow channels" (Stripa experiments, inflow to the Äspö tunnel, High Permeability Features project, etc). Based on these experiences we assume that there is one major flow channel, providing perhaps more than 90 % of the total flow, and a number of secondary flow channels with a much weaker flow (marked *C* in the figure). These secondary channels and possible cavities with circulation, *D*, give advective exchange with more or less stagnant water (compare "Miller's advective immobile exchange approach"). It is important to note that the secondary channels may be very effective for retarding a tracer; both because they have a much lower velocity but also because they expose the tracer to larger volumes of truly stagnant water. Hence the "diffusive interface" can be significantly enlarged.

The main flow channel may be connected to other flow channels within the fracture (marked *E*) or to the three dimensional fracture network, *F*. The influence of these may not be very significant if the pressure gradient is aligned with the main flow channel and everything is at a steady state. Most interpretations of tracer transport and retardation assume steady state conditions and this may be correct for an experiment with a pumped borehole as the local pressure gradients are determined by the pumping. For natural conditions (and long time scales) this assumption may however be questioned. It is easy to find transient processes on a wide range of time scales that can generate fluctuations (tidal effects, sea level variations, seasonal variations in precipitation, etc). It is unlikely that these will give rise to a perfectly uniform variation in pressure; instead one can expect time dependent pressure gradients and hence flow to develop.

It is here argued that transient effects may be important to consider when long term transport under natural conditions is studied. In Figure 2-4, the crossing fractures (*F*) and the connected channel (*E*) may be activated and displace a tracer cloud significantly in the transverse direction. Also minor displacements from the main channel may be important as a small advective transport is often more effective than purely diffusive exchange.

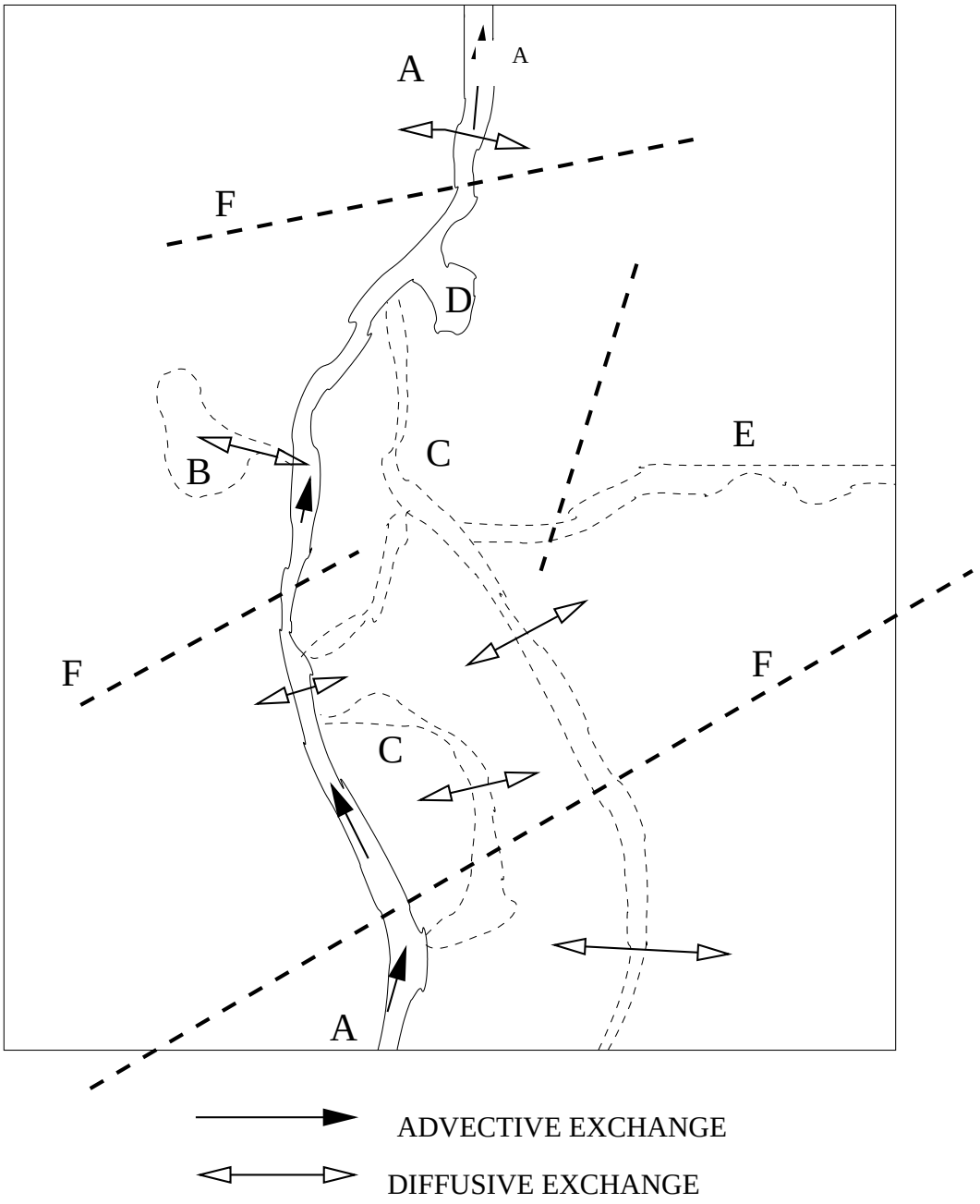

A. Main flow channel.

B. Stagnant pool exchanging mass by diffusion only (dead end volume).

C. Secondary flow channel.

D. Pool of water with advective exchange.

E. Flow channel which may be activated due to a transverse pressure pulse.

F. Crossing fracture that may provide a flow channel and connect the main flow channel to the three dimensional fracture network.

Figure 2-4. *Conceptual view of exchange processes in a fracture plane.*

This will be demonstrated in a simulation later in this report. The arguments put forward can be considered as an extension of "Miller's advective immobile exchange approach", by also including transient effects.

2.4 Concluding remarks

From the above discussion it is not possible to formulate a consensus about the geometry and retention properties of a fracture; not even Feature A. It is likely (see Bossart et al., 2001) that fractures have to be treated by a type classification with respect to, for example, size and mineralogy.

The discussion provided can be summarized as:

- Fracture anatomy with respect to geometry (for example parallel flow channels) and mineralogical composition is uncertain.
- Many retention processes are conceivable; it is difficult to conclude which are dominating in a particular experiment.
- Stagnant or near-stagnant water in the fracture plane may be more important than earlier anticipated; especially so for "natural conditions with transients".

These points apply both to Feature A and generally.

3 Modelling approach

3.1 Introduction

It is clear from the previous section that large uncertainties remain, concerning the geometry and retention processes in Feature A. If a simulation model is to be set up for the problem, two alternative approaches can be followed:

1. Start with the simplest possible model and add features as evidence and needs come along.

2. Formulate a more general model that is not specific to a certain experiment and the information collected in this experiment.

In this study the second approach has been adopted. One reason for this is that we are going to use the computer code DarcyTools (Svensson et al., 2004) which has some of the features required for these simulations already built in. The argument is however not "we take what we have"; instead we believe that the concepts and methods embodied in DarcyTools are particularly useful in this study and in the continuation of Task 6, where long term transport simulations in three dimensional fracture networks are requested.

It is beyond the scope of the present report to describe DarcyTools; instead the reader is referred to Svensson et al. (2004). It needs however to be stated that DarcyTools is a finite-volume code. To handle subgrid processes, i.e. processes with a length scale smaller than the cell size, a subgrid model called FRAME has been developed. FRAME is developed for both advection/diffusion equations (used for salinity) and particle tracking, which is to be used in this study. The particle tracking algorithm in DarcyTools is called PARTRACK.

3.2 Frame – an outline

In Figure 3-1 some subgrid processes and concepts are introduced. Let us consider a computational cell with a through flow, i.e. a cell with a flow channel. The flow "sees" a certain surface area, the flow wetted surface (FWS), as it passes the cell. The FWS may bring the flowing water in contact with other fractures, gouge material, stagnant pools, etc. Most of these volumes can be expected to have stagnant water and mass exchange is hence due to molecular diffusion. For a stagnant pool the relevant diffusion coefficient may be that for pure water, while diffusion into crossing fractures and the rock matrix may proceed with a diffusion rate that is several orders of magnitude smaller. In the following we will call the volume with flowing water the mobile zone and the volumes with no advection the immobile zone. Fractures and volumes which are not in contact with the mobile zone are of course of no relevance and can be excluded from the discussion.

The situation outlined in Figure 3-1 is quite complicated and does not lend itself to direct descriptions of individual processes. In order to derive a simple model that can be employed in large (many grid cells) 3D models, the following basic assumption will be made:

- The immobile zones can be represented by a set of boxes, each with its own length scale, volume and effective diffusion coefficient.

The idealised problem is illustrated in Figure 3-2. The box with the smallest length-scale (dimension perpendicular to the mobile zone) will have the largest diffusion coefficient and normally also the largest contact area with the mobile zone. This volume will hence have a fast response. The actual response time can be estimated from the length scale, *l*, and the effective diffusion coefficient, D_e, as:

$$t \approx \frac{l^2}{D_e}$$

For $l = 10^{-3}$ m and $D_e = 10^{-10}$ m^2/s the time is 10^4 s $(\approx 3\,\text{hours})$. For *l*= 1 m and $D_e = 10^{-12}$ m^2/s the time will be 10^{12} s (30 000 years), which illustrates that both short and long time scales may be treated within the same concept. In the following we will call these boxes storage volumes, which thus represent an idealised view of the immobile zones.

The next step is to devise methods to calculate the FWS, storage volumes, diffusion coefficients, etc. Fractal scaling laws will be used in this context and as we have adopted a multirate diffusion approach we call the subgrid model FRAME (a subgrid model based on FRActal scaling laws and Multirate Equations). Methods to derive the FWS are described in detail in Svensson et al. (2004), and here we will focus on the properties of the storage volumes. The following steps will determine these:

- Divide the immobile volumes, illustrated in Figure 3-2, into a number of size groups with respect to the length-scale.
- Generate the number of fractures in each size group from a power-law with exponent D_f. Note that the same power-law as used for the resolved fracture network is used also for the subgrid system. This will give the number of fractures per m^3, for the size group in question.
- Only immobile zones in contact with the FWS can be in contact with the flowing water. Modify the number of fractures in each size group with respect to this constraint.
- Assume that the aperture of a fracture is proportional to the length scale, i.e. $e_T \sim l^{\gamma}$. Note that for $l >> l_{\min}$, it can be expected that the immobile zones are due to fractures. For $l \approx l_{\min}$ the volumes are perhaps due to stagnant pools and it may be questionable to speak about an aperture.
- The effective diffusion coefficient, D_e, is expected to be close to the molecular value for water, D_w, for the smallest volumes and then show a decreasing trend with the length scale of the immobile zone. The following relation is assumed:

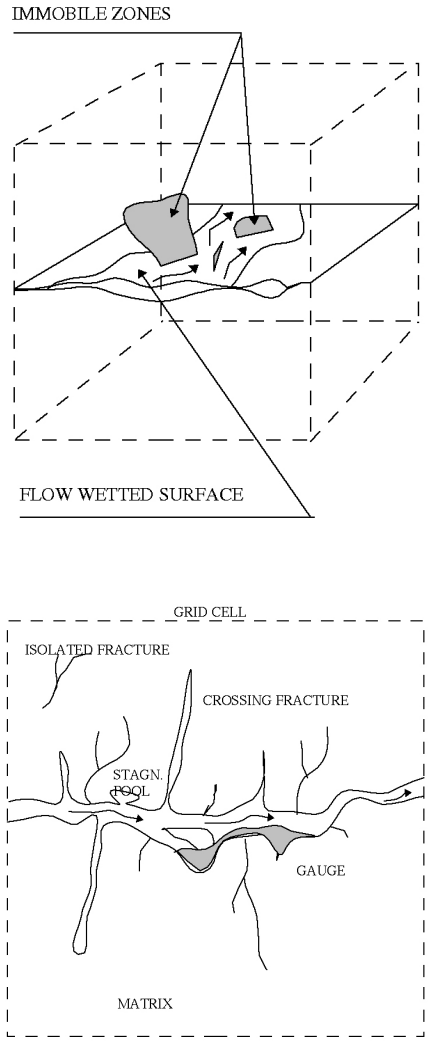

Figure 3-1. *Illustration of subgrid processes and concepts.*

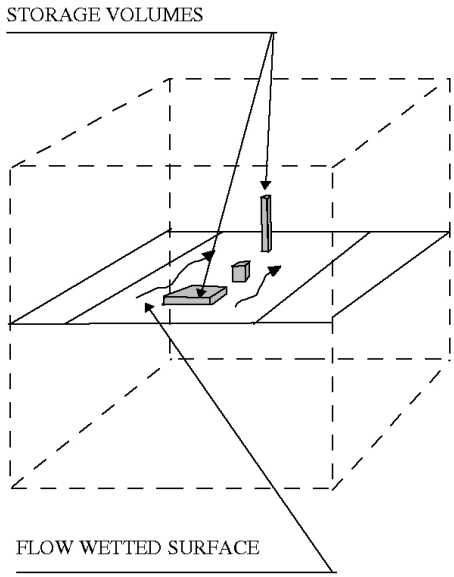

Figure 3-2. *The assumed structure of subgrid volumes and areas.*

$$D_e = D_w \left(\frac{l}{l_{\min}} \right)^{\Psi}$$

By these steps the volume, contact area and effective diffusion coefficient have been determined for each storage volume, as a function of D_f, γ and Ψ. However, these parameters will not be specified individually as they can be related to the "late time slope of the breakthrough curve"; this will be further discussed below.

Regarding the size interval to be considered, it was shown above that a length scale of 10^{-3} m results in a storage volume that has a response time of the order of a few hours. Smaller, or faster, boxes are probably not required, unless a very fast experiment is to be simulated. The upper limit should be the cell size, Δ, as larger fractures are normally treated explicitly in the resolved fracture network. However, Δ is often in the range 1-10 metres and the largest storage volume will hence be very slow. From a practical point of view (save computer time) the upper limit may hence be chosen with respect to the time scale of the problem considered. Note also that fractures in the resolved network may form dead-end systems that exchange matter with the flowing water by molecular diffusion only.

The concepts and assumptions introduced give a very simplified view of the expected subgrid processes. However, it should be remembered that the objective is to derive a subgrid model that can be employed in large 3D, transient models. It is hoped that FRAME strikes a good balance between complexity and efficiency.

3.3 Frame – some further development

As discussed above, FRAME is based on a power-law formulation. The main argument for this is that the fractal properties of the subgrid fracture network should be the same as for the resolved network. The use of a power-law formulation does however also support a further development of the model.

- In the multirate diffusion model each storage volume is represented by a series of first order capacity boxes. When all storage volumes have been represented, the continuous distribution of capacities is also a power-law. This can be shown both numerically and analytically.
- It can further be shown that the slope of this distribution is related to the late time slope of the breakthrough curve, *k*.
- Above the properties of the storage volumes were stated to be a function of three parameters: D_f, γ and Ψ. It can be shown, see Svensson et al. (2004), that these are related to *k* as follows:

$$k = \frac{D_f - \gamma - 2\Psi + 1}{2 - \Psi}$$

These developments form the basis for the implementation of FRAME. We thus specify the distribution of capacity boxes, with their associated mass transfer coefficients.

The parameters that specify this model are k, β_t and D_m (retention coefficients R_m and R_{im}, are also needed for a sorbing tracer), where β_t denotes the ratio between the immobile and mobile volumes averaged over the whole domain. The FWS is also needed to consider in applications were a cell to cell variation of FWS is taken into account. The method employed is to calculate a β_t that varies from cell to cell. This is done by using FWS/vol_m (where vol_m is the volume of the mobile zone) as a weighting factor and then ensure that the global mean of β_t has the prescribed value.

Thus:

$$\beta_{t,cell} = \overline{\beta}_{t,cell} \left(\frac{FWS}{vol_m} \right)_{cell} / \left(\frac{\sum FWS}{\sum vol_m} \right)$$

where overbars indicate a global average.

3.4 Summing up

It is of course a prerequisite that the flow rate through the cell is known, as well as the FWS, when the retention due to the storage volumes is to be calculated.

The FRAME parameters that control the retention effect are:

- β_t, the capacity ratio between the immobile and mobile zones.
- k, the late time slope of the breakthrough curve (BTC). As shown, k is related to the properties of the storage volumes.
- D_w, molecular diffusion coefficient in water.
- $\alpha_{\min}$ and $\alpha_{\max}$ that specify the limits of the mass transfer coefficients. These are related to length scales and diffusion coefficients.
- R_m and R_{im}, retardation factors for the mobile and immobile zones respectively. These parameters are only needed for sorbing tracers.

4 Results

4.1 Verification, sensitivity studies and validation

As DarcyTools, FRAME and PARTRACK have not earlier been used to simulate tracer transport experiments, some basic evaluations of the methods are needed. The details of these are given in the appendices; her only a brief summary is provided.

Verification

The objective of the verification study is to demonstrate that the numerical model results agree with the analytical solution for a single rate diffusion problem. The analytical solution for an infinite matrix is well known (Neretnieks (2002), Barten (1996), Cvetkovic et al. (1999), etc). The numerical model was set up for such a case and various cases, changing parameters and parameter groups, were then evaluated. All results are in good agreement with the corresponding analytical solution. For further details see Appendix A.

Sensitivity studies

When calibrating a model, it is useful to know how different parameters affect the predicted outcome, in this case the BTC. For this purpose, a reference case was first specified and key parameters were then varied in a systematic manner. The selected parameters are: $l_{\min}$ (smallest capacity box), R_m, R_{im}, β_t and k. A brief statement of the results is: "$l_{\min}$ does not affect the BTC significantly", "R_m causes a delay of the BTC" and "R_{im}, β_t and k all increase the retention when increased". For further details see Appendix B.

Validation

Validation implies that the simulations should be compared with measurements. However, in this study a "somewhat derived form" of the field data will be used. The BTC:s measured in field have been deconvoluted to a unit response function, i.e. the BTC that represents the expected result from a Dirac pulse input (see Elert and Svensson, 1999). For the present purpose we will however regard the deconvoluted BTC as field data.

The objective of the validation study is to show that the numerical model can be tuned to fit the experimental BTC:s. It is however not meaningful to use all model parameters in such a tuning or to use unrealistic values on parameters. In Appendix C the arguments for the chosen strategy are given and results are discussed.

The general conclusion of the validation study is that fair agreement with measured BTC:s can be achieved for non sorbing and weakly sorbing tracers, but less satisfactory agreement is found for strongly sorbing tracers. This with model parameters that can be regarded as plausible from a physical point of view.

4.2 Task 6A

Problem specification

This task concerns a field experiment carried out in Feature A (STT1b in Figure 2-1). The length of the flow channel is estimated to 5.03 and the aperture to 1 mm. These are the values used in the simulations. The case is treated as a one dimensional channel flow, with a constant velocity of 7×10^{-4} m/s (based on the first arrival of a tracer, see Figure 4-7 in Elert and Svensson, 2001).

The tracers modelled are iodine, strontium, cobalt, technetium and americium. Property data specified for these are summarised in Table 4-1. The R_m and R_{im} values used are according to the K_a and K_d values and the formulae given in Table 4-1. The exception is strontium where the validation study indicated that somewhat modified values improved the agreement with field data. Values within brackets give the values from the input data.

Several model parameters need to be set before simulations can be carried out. The strategy for this specification follows from the second part of the validation study, meaning that:

- k is fixed to 2.0.
- β_t is equal to 10.0 for a non sorbing tracer, β_n, and equal to $\beta_n R_{im} / R_m$ for sorbing tracers.
- Note: $\beta_t = \frac{R_{im}V_{im}}{R_m V_m} = \frac{R_{im}}{R_m}\beta_n$, where V_{im} and V_m are the volumes of the immobile and mobile zones, respectively.
- $\alpha_{\min} = 10^{-10}$ for HTO and equal to $\frac{D_w}{R_{im}D_{w,HTO}}\times10^{-10}$ for other tracers.
- $\alpha_{\max}$ is based on an average between $D_w / l_{\min}^2$ and $D_w / \left(l_{\min}^2 R_{im}\right)$, see Appendix C.
- $l_{\min}$ is put to 10^{-3} (equal to the aperture).

A further comment may be needed on the specification of $\alpha_{\max}$. A key uncertainty, see Section 2.3, concerns the role of the stagnant water in the fracture plane. As $\alpha_{\max}$ is the mass transfer rate for the fastest (smallest) capacity boxes, one may argue that $\alpha_{\max}$ should represent exchange with stagnant water. If so $\alpha_{\max}$ should be set to $D_w / l_{\min}^2$. However, if the smallest boxes represent exchange with the matrix $\alpha_{\max}$ should be set to $D_w / \left(l_{\min}^2 R_{im}\right)$. In the validation study an average, based on the $\log_{10}$ values, was suggested and evaluated. For Task 6A we use the average as a base; however for cobalt it was found (see Appendix C) to improve agreement to use a lower value; this lower value is used also for Task 6A.

Simulation results

Breakthrough curves for a Dirac pulse are shown in Figure 4-1 and for a continuous injection in Figure 4-2. Breakthrough times for a recovery of 5, 50 and 95 % of the injected mass can be found in Table 4-2.

Based on the result for rubidium and cobalt, see Appendix C, one can expect that $\alpha_{\max}$, based on the averaging procedure discussed, for technetium and americium is too high. A smaller value would give an earlier first arrival, while the final part of the BTC would remain the same.

Table 4-1. Tracer property data (Based on the Task 6 specification, Selroos and Elert, 2002).

Tracer	D_w $(\times 10^{-9})$ [m^2/s]	K_a [m]	K_d [m^3/kg]	R_m	R_{im}
Iodine	1.66	0	0	1	1
Strontium	0.78	8×10^{-6}	4.7×10^{-6}	2.5 (1.02)	2.0 (4.2)
Cobalt	0.5	8×10^{-3}	8×10^{-4}	17	542
Technetium	0.78	0.2	0.2	401	1.35×10^{5}
Americium	0.78	0.5	0.5	1001	3.38×10^{5}

$$R_m = 1 + \frac{2K_a}{e_T}, \quad R_{im} = 1 + \frac{2700K_d}{0.004}$$

Table 4.2. Breakthrough times (in hours) for recovery (in%).

Tracer	$t_{5\%}$	$t_{50\%}$	$t_{95\%}$
Iodine	1.9	5.3	29.4
Strontium	4.7 139.	10.6 1.4×10^3	58.3 1.1×10^4
Cobalt	4.4×10^5 1.3×10^6	9.2×10^5 2.4×10^6	3.3×10^6 8.1×10^6
Technetium			
Americium			

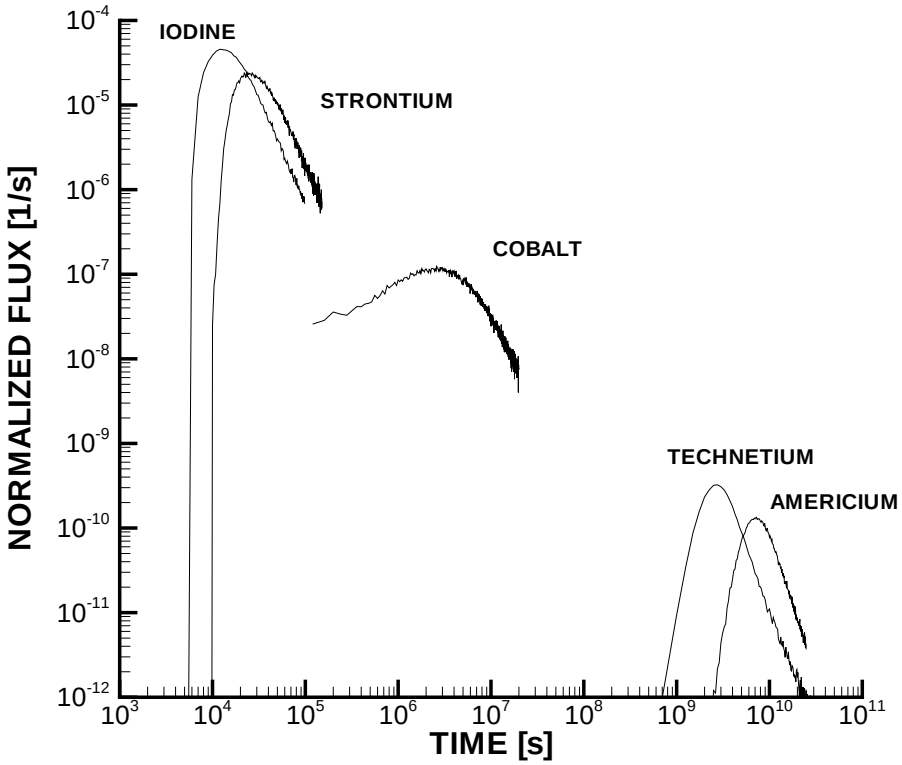

Figure 4-1. *Task 6A. BTC:s for a Dirac pulse.*

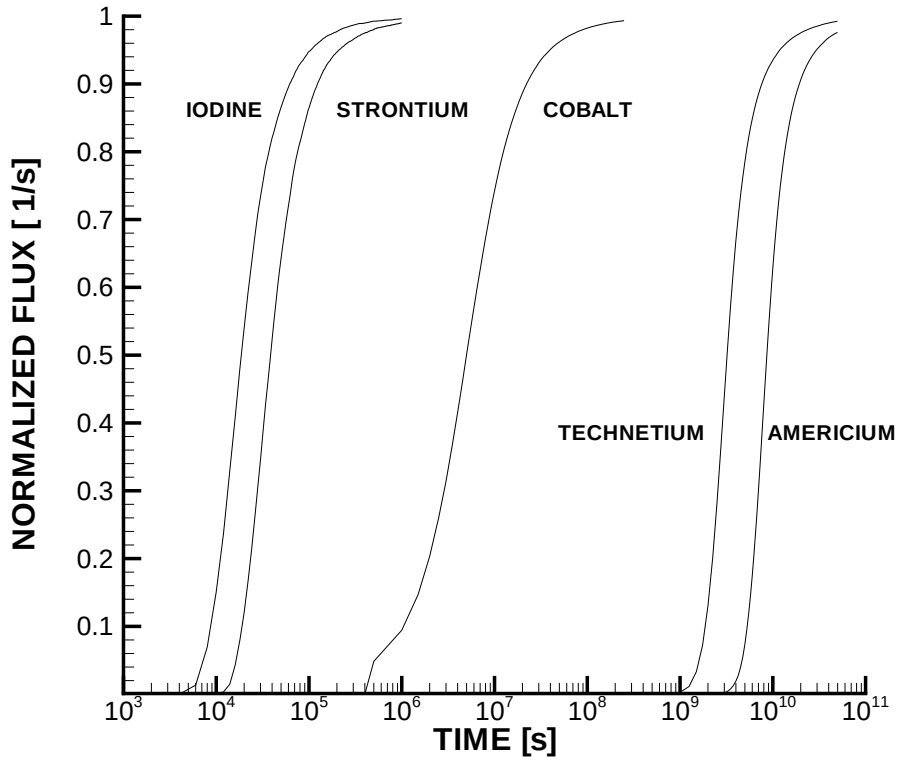

Figure 4-2. *Task 6A. BTC:s for continuous injection.*

4.3 Task 6B

Problem specification

Task 6B is intended to demonstrate what happens under natural conditions, i.e. if the flow rate is significantly lower (as compared to 6A). All other conditions are the same as for Task 6A.

As the simulation is one dimensional with a specified flow velocity, the only change in the input specification is a reduction of the velocity with a factor of 1000.

Simulation results

Breakthrough curves for a Dirac pulse are shown in Figure 4-3 and for a continuous injection in Figure 4-4. Breakthrough times for a recovery of 5, 50 and 95 % of the injected mass can be found in Table 4-3.

The same comment about α_{max}, as given for Task 6A, applies also for this case.

Table 4-3. Breakthrough times (in years) for recovery (in %).

Tracer	$t_{5\%}$	$t_{50\%}$	$t_{95\%}$
Iodine	1.0	1.5	4.4
Strontium	2.3	3.0	8.4
Cobalt	390	550	1680
Technetium	1.7×10^{5}	2.2×10^{5}	5.2×10^{5}
Americium	4.0×10^{5}	5.2×10^{5}	1.3×10^{6}

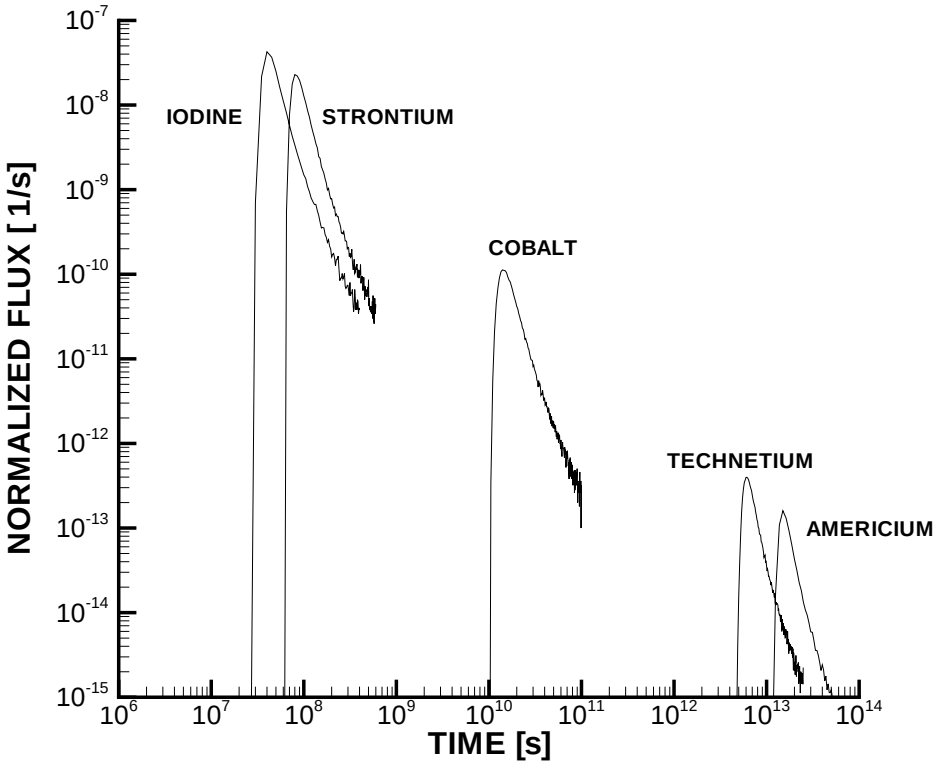

Figure 4-3. *Task 6B. BTC:s for a Dirac pulse.*

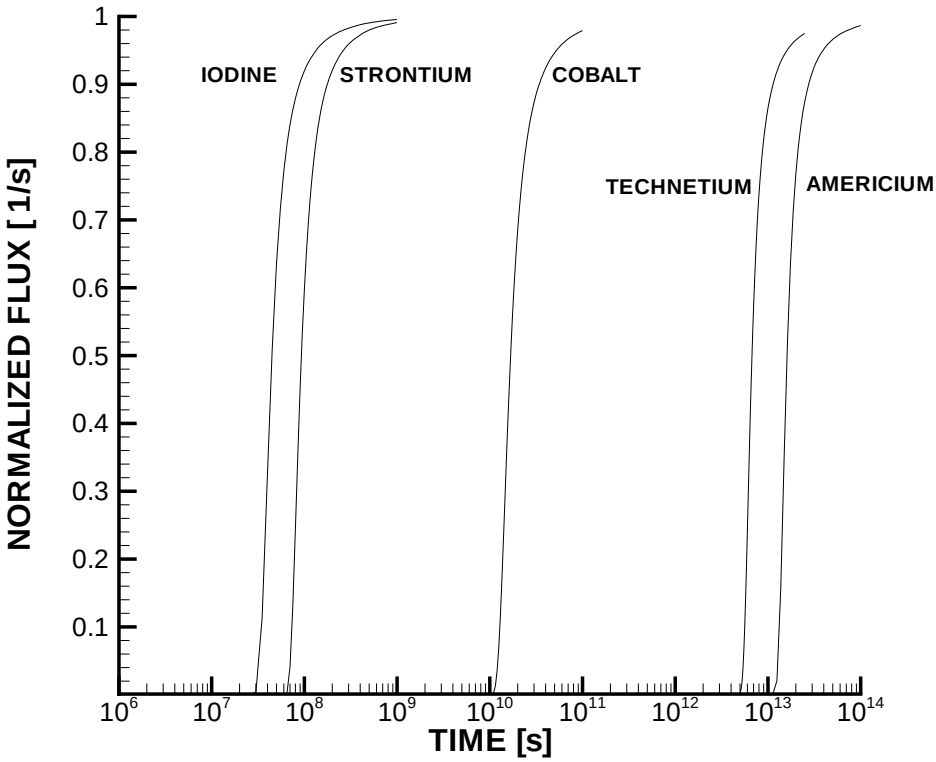

Figure 4-4. *Task 6B. BTC:s for continuous injection.*

4.4 Task 6B2

Problem specification

Task 6B2 aims to study transport from a line source, see Figure 2-1. Account should also be taken of the heterogeneity of the transmissivity field. The problem could be solved as a two dimensional one; however in order to test some advanced features of DarcyTools and prepare for future tasks within Task 6, a fully three dimensional analysis will be carried out. The three dimensionality is introduced by a 3D fracture network that is in contact with Feature A. Figure 4-5 gives an outline of the problem. The problem specification is given by this figure and the following points:

- A head difference between the inlet and outlet plane of 0.015 m is specified; all other boundaries are of the zero flux type.
- The transmissivity of Feature A has a typical range of $0.8 \rightarrow 40 \times 10^{-8}$ m^2/s, with a correlation length of $0.3 \rightarrow 0.4$ m.
- Tracer specification as for Task 6A and 6B.
- The line source has a length of 2 metres.

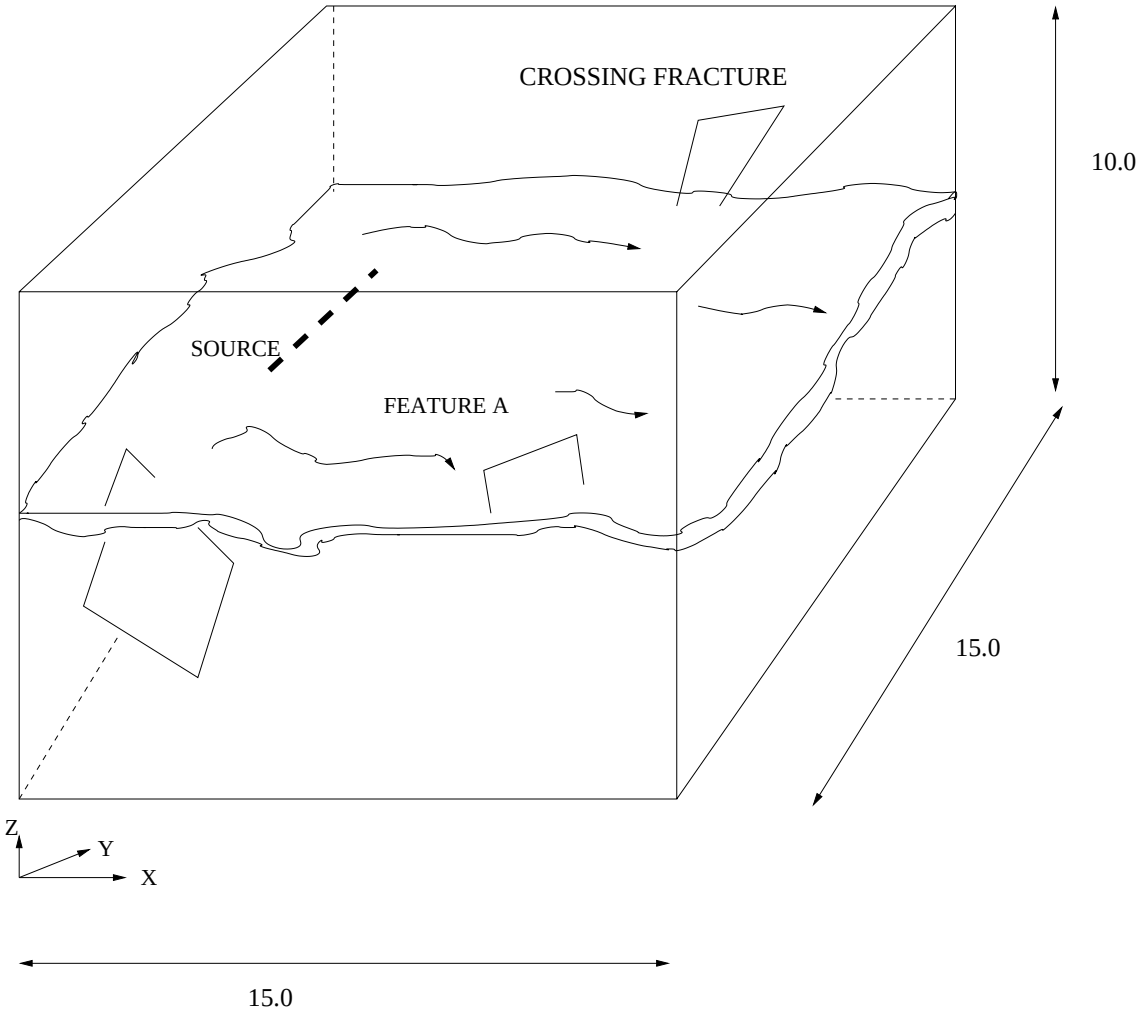

Figure 4-5. *Task 6B2. Outline of situation studied.*

Model input data

The approach chosen involves a 3D grid in which a fracture network is to be represented as conductivities, porosities, flow wetted surface, etc. Once again the reader is referred to the DarcyTools documentation (Svensson et al., 2004) for details. However, some aspects of the methods and concepts will be discussed here as they are needed as a background for the discussion of results.

The 3D grid has a cell size of 0.2 metre, resulting in a grid with 281 250 cells (75 x 75 x 50). A fracture network with the largest fracture equal to 10 metres and the smallest equal to 0.2 metre is generated. All fractures and fracture groups not in contact with Feature A are removed as they can not contribute to flow or transport. The final result is summarised in Table 4-3.

Table 4-3. The stochastic fracture network.

Set	Average size (m)	Number	FWS (m^2)	e_T $(\times 10^{-4})$ (m)	Volume $(\times 10^{-3})$ (m^3)
1	7.	1	98	0.82	4.1
2	4.	10	320	0.42	6.7
3	2.	31	248	0.18	2.2
4	1.0	83	166	0.08	1.3
5	0.5	296	148	0.04	0.3
6	0.25	970	121	0.02	0.1
			Σ 1101		$\Sigma 1.5\times10^{-2}$

As can be seen the fractures are subdivided into six sets with respect to size. The number of fractures in each set comes from the generation (one realisation). It is then easy to calculate the total FWS and the volume for each size group. We then use the formulae given in the DarcyTools report to calculate the thickness (b), transmissivity (T), aperture (e_T) and porosity (n). It is then possible to estimate the volume contribution from each size group. The final result of the analysis is the total FWS and volume that are due to the stochastic fracture network (Feature A not included).

For Feature A we can estimate:

- Volume $= 15\times15\times10^{-3} = 22.5\times10^{-2}$ m^3
- FWS $= 2\times15\times15 = 450$ m^2

By comparing these figures with the corresponding for the stochastic fracture network, we may conclude:

- The total volume of the immobile zone will largely be determined by Feature A as this volume is much larger than the volume from Table 4-3. Note that the immobile volume is calculated from the specific β_n and the volume of the mobile zone.
- On the cell scale β is made proportional to the local FWS. As the FWS is mainly found in the background fractures, most of the immobile volume will be connected to these fractures.

We may also estimate the total porosity in the connected volumes (isolated fractures have been removed). Assume that $\beta_n = 10$; we then have

Feature A	22.5×10^{-2}
Stochastic fractures	1.5×10^{-2}
Immobile volumes	$\underline{240\times10^{-2}}$
	248×10^{-2} m^3

The total connected porosity is hence $\left(248\times10^{-2}\right)/\left(15\times15\times10\right)=1.1\times10^{-3}$ and the porosity of the mobile volumes roughly one order of magnitude smaller. These figures seem reasonable.

This exercise demonstrates that DarcyTools and FRAME allow a very detailed description of the fracture system, both mobile and immobile. It also outlines (many details are left out) how the concepts work in a fully three dimensional case.

Simulation results

Both the transmissivity variation in Feature A and the three dimensional fracture network are generated stochastically. In order to illustrate this, three realisations of these fields will be generated and used in the flow and transport simulations.

Three fracture networks are shown in Figure 4-6. It should be pointed out that the fractures that look like they were isolated are connected to one of the boundaries. A decision was taken that "fractures connected to the boundaries should not be removed, when isolated fractures are sorted out, as we can not for certain say that these are isolated". All other fractures are connected to Feature A, directly or through another fracture.

The corresponding flow fields in Feature A are shown in Figure 4-7. The strength of the channelling is specified with the given variation of the transmissivity field ($T = 0.8 \rightarrow 40\times10^{-8}$ m^2/s, with a correlation length of 0.4 m). DarcyTools allows for an anisotropic specification; however an isotropic distribution was used for the present case.

Breakthrough curves for the five tracers can be found in Figures 4-8 (Dirac pulse) and 4-9 (continuous injection). It is interesting to note that double peaks are present in all three realisations. For a line source it is of course not surprising that the effect of multiple flow paths is prominent.

The FWS is specified for each fracture in the network; for stochastic fractures each set is given a value, for deterministic features an individual specification is used. For Feature A a value of 2 m^2/ m^2 (giving a total area of 450 m^2) was specified. If several parallel flow channels in a fracture are present a higher value can be specified. In Figure 4-10 the effect of specifying 8 m^2/ m^2 for feature A can be studied. To understand the result one should note that "more FWS in a cell results in larger immobile volumes", according to the methods employed. In the problem specification above, it was found that the FWS in Feature A was 450 m^2 and 1101 m^2 in the stochastic fractures. By increasing the FWS in Feature A with a factor of four, we move immobile volumes to Feature A. The total ratio, β, should of course be constant in this test. From this explanation one can expect the result displayed in Figure 4-10, as most of the tracer will stay in Feature A, which now has more immobile volumes connected.

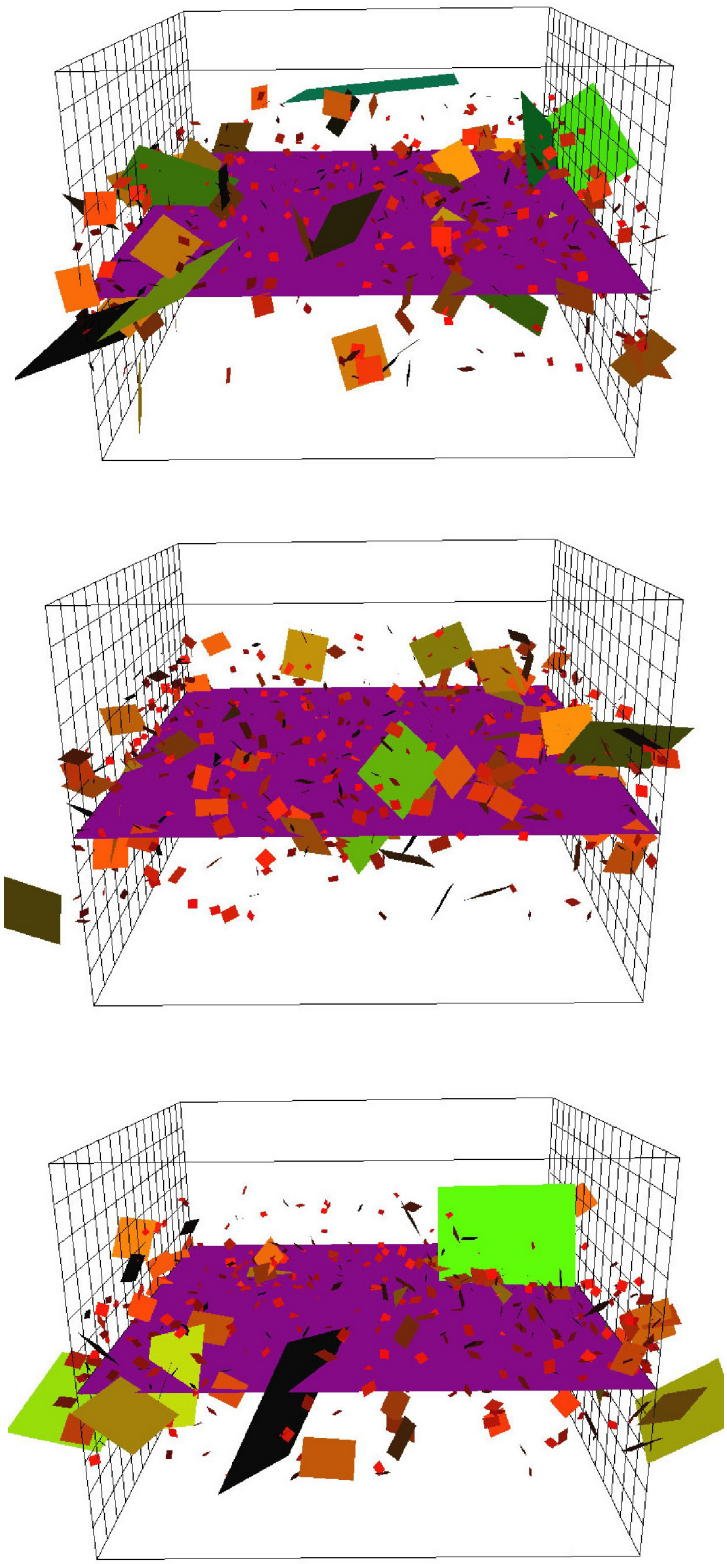

Figure 4-6. *Task 6B2. Three realisations of the fracture network that is connected to Feature A (purple in the figure). Inlet and outlet planes are marked with a grid.*

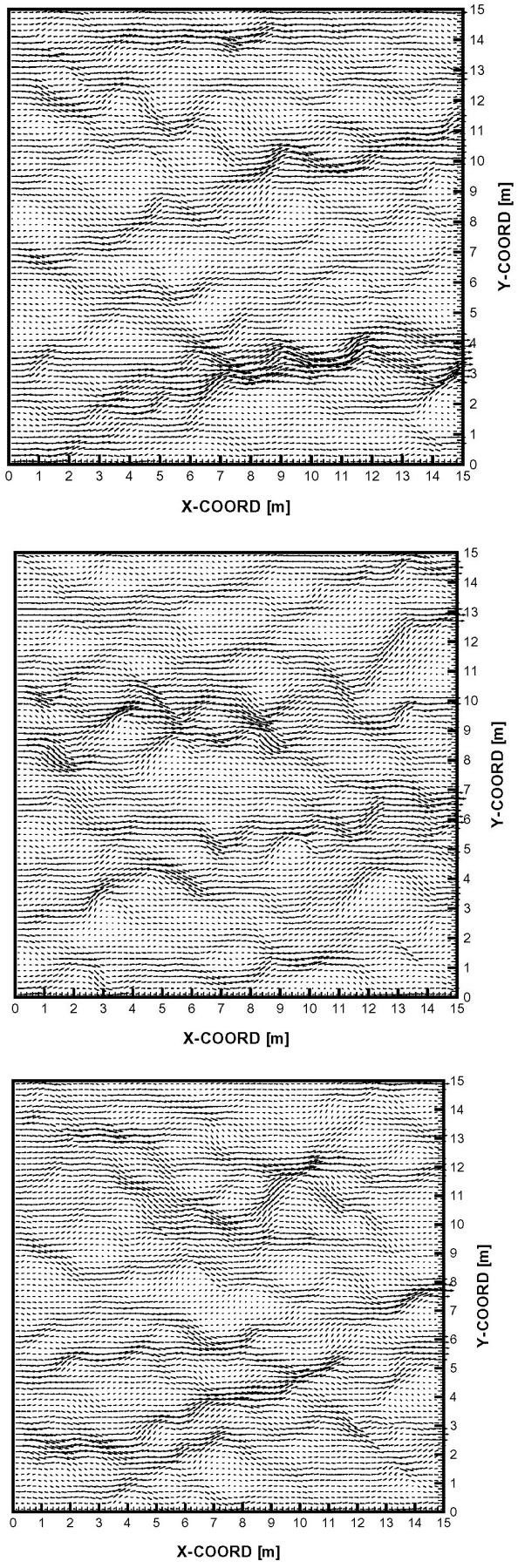

Figure 4-7. *Task 6B2. Three realisations of the flow field in Feature A.*

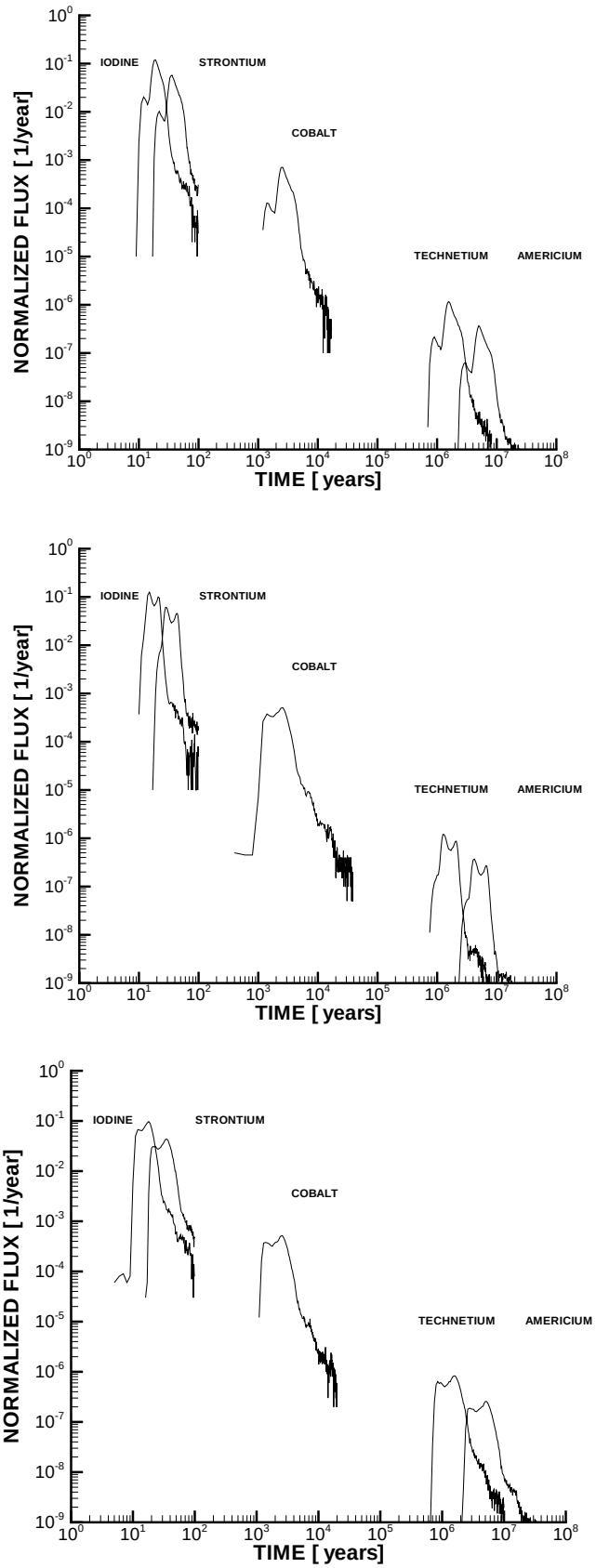

Figure 4-8. *Task 6B2. BTC:s for a Dirac pulse. Three realisations of the fracture network.*

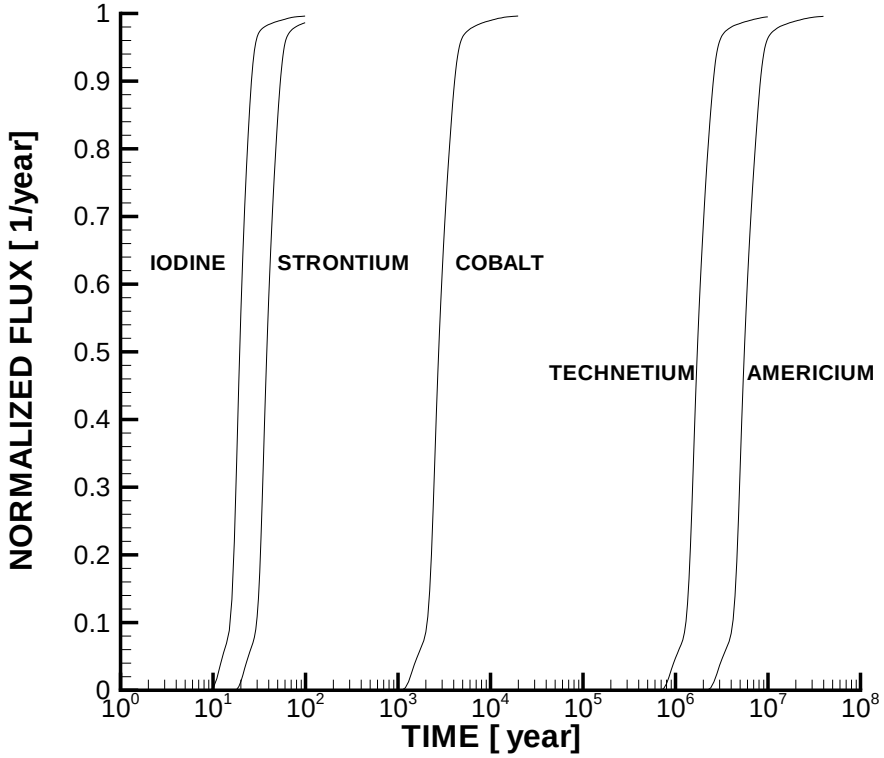

Figure 4-9. *Task 6B2. BTC:s for a continuous injection.*

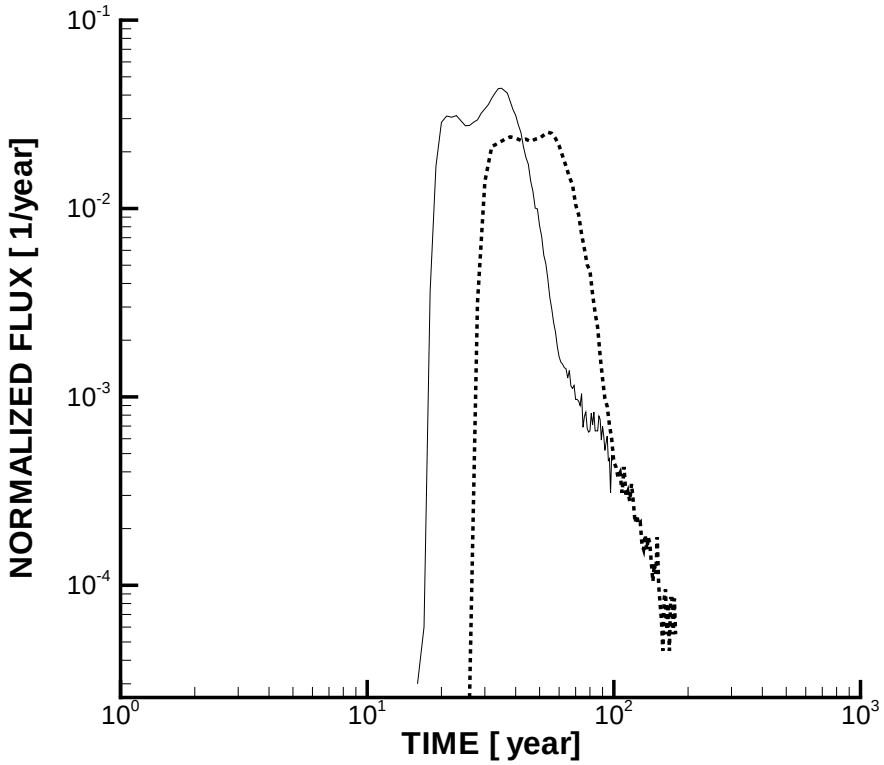

Figure 4-10. *Task 6B2. BTC:s for strontium based on a FWS equal to 2 m^2/m^2 (solid line) and 8 m^2/m^2 in Feature A.*

4.5 Transients

Problem specification

In Section 2 the possible retention effect of near stagnant water and transients was discussed. We will now continue this discussion by studying the effects in a simple generic test case.

The starting point is the simulation of strontium in Task 6A, see above. The basic specification (including retention parameters) is thus exactly as this case, but now the problem is specified as a two dimensional one, see Figure 4-11. The one dimensional channel used in Task 6A is found along the centreline; this channel has a constant velocity u. The adjacent volumes have a velocity $f \times u$ and a transverse time dependent velocity v acts uniformly over the whole fracture plane.

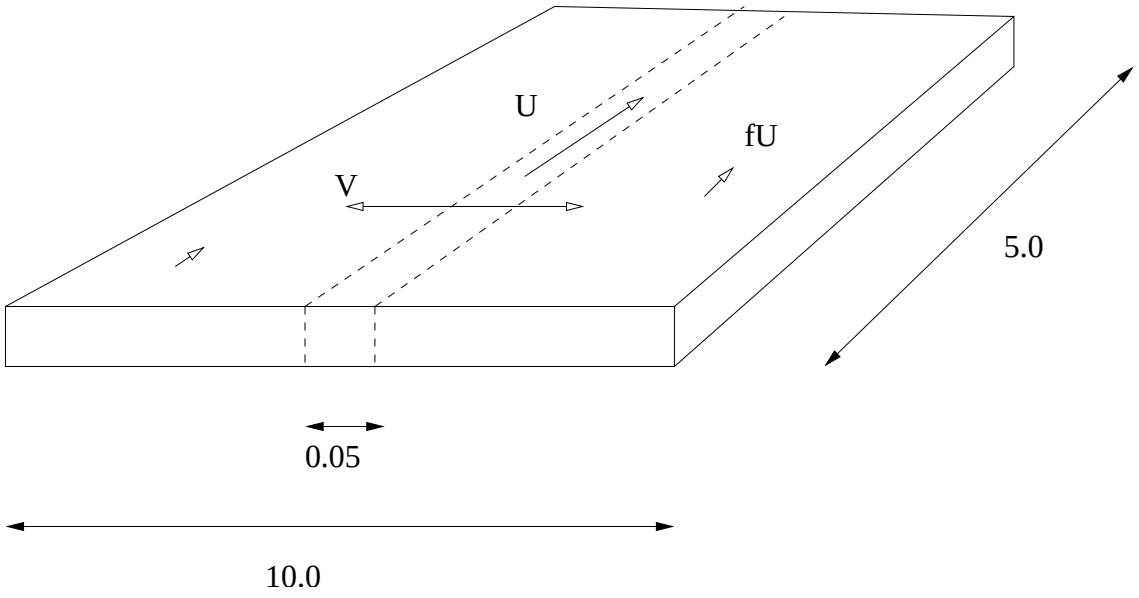

Figure 4-11. *Transients. Outline of situation studied.*

The tracer pulse is injected in the central channel but will be displaced into the adjacent volumes by the transverse velocity. Due to several processes (Taylor dispersion, matrix diffusion and sorption) some of the tracer will however stay in the slowly moving water and perhaps never find its way back to the central channel. This process will affect the BTC.

Model input data

The problem is specified by Task 6A and Figure 4-11. The transverse velocity is specified by:

$$v = v_{\max} \sin(2\pi t / t_w) \qquad (4\text{-}1)$$

where $v_{\max}$ is the maximum velocity, t time and t_w the advective travel time (L/u). The following variations will be tested:

$v_{\max} = 0.1u$ and $0.5u$

$f = 1.0$, 0.1 and 0.01

$v_{\max} = 0.5u$ gives an excursion length of about 0.5 m during one period. As some particles are left at this position and may be displaced further away during the next period, one realises that particles can be displaced any distance from the centre line.

Simulation results

BTC:s for the two $v_{\max}$ values tested are shown in Figure 4-12. For $f = 1.0$ there is no effect as the BTC is in agreement with the measurements (as in Task 6A). For $f = 0.1$ and 0.01, the effect is very strong indeed.

It is not surprising that the transverse velocity retards the particles as they simply experience a lower forward velocity, when in the near stagnant water. The particle distributions at time 3×10^5 s are shown in Figure 4-13 $(v_{\max} = 0.5u)$ and Figure 4-14 $(v_{\max} = 0.1u)$. As can be seen, the particles have been displaced several metres by the oscillating velocity.

Concluding remarks

The strong effect of an oscillating transverse velocity is easy to understand in this simple generic test case. The more difficult question is whether we can expect such effects in a real world case.

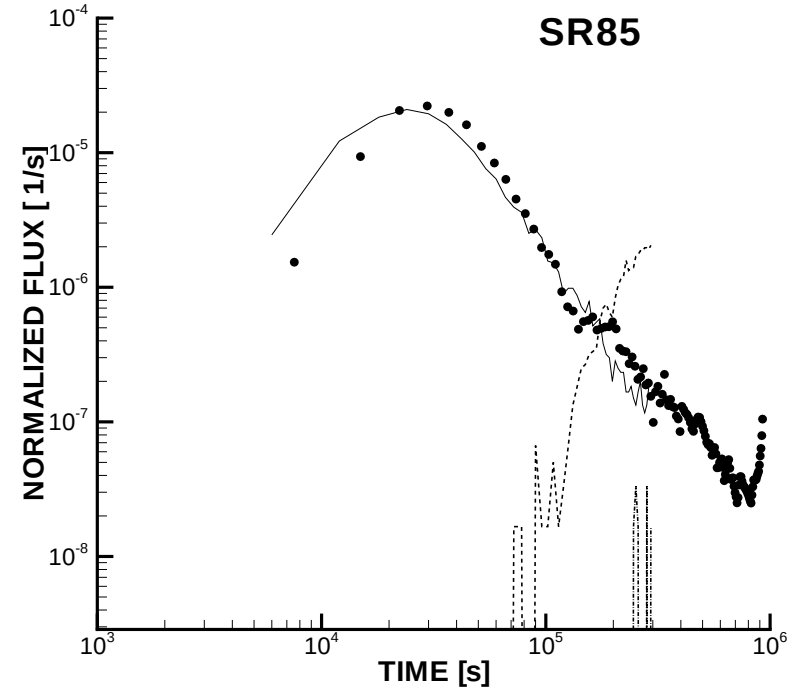

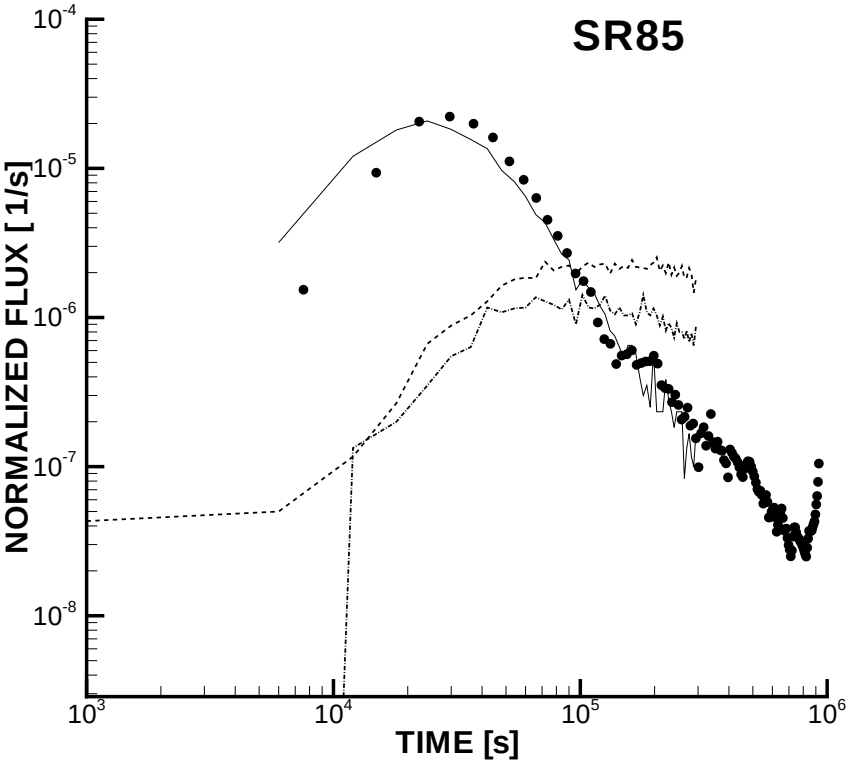

Figure 4-12. *Transients. BTC:s for* $v_{\max} = 0.5u$ *(top) and* $0.1u$ *. Velocity in adjacent volume specified to 1.0 (solid), 0.1 (dash) and 0.01 (dash-dot). Dots represent measurements.*

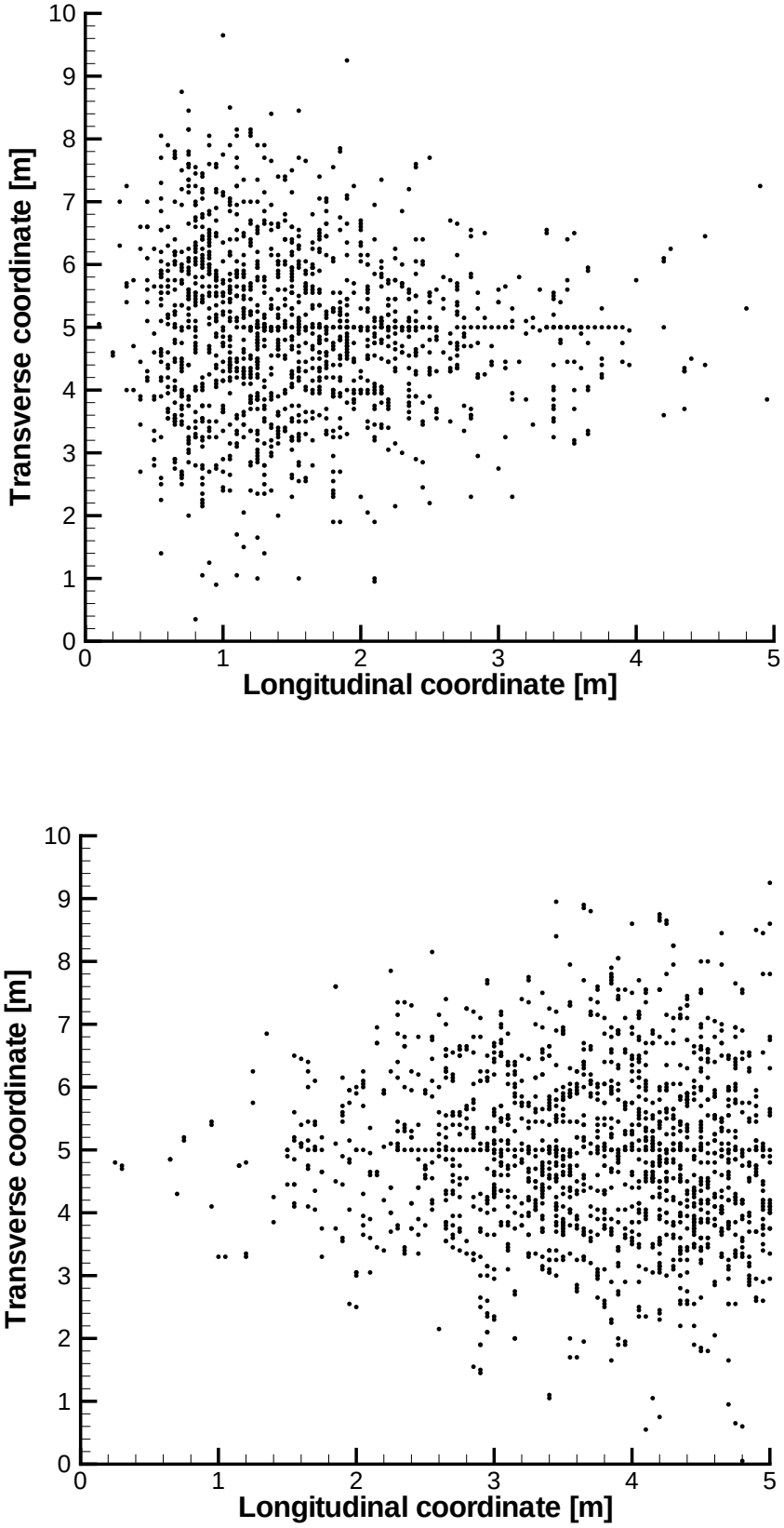

Figure 4-13. *Transients. Particle distribution at time* $3\times10^5 s$*, for* $f = 0.01$ *(top) and* $f = 0.1$*.* $v_{\max} = 0.5u$*.*

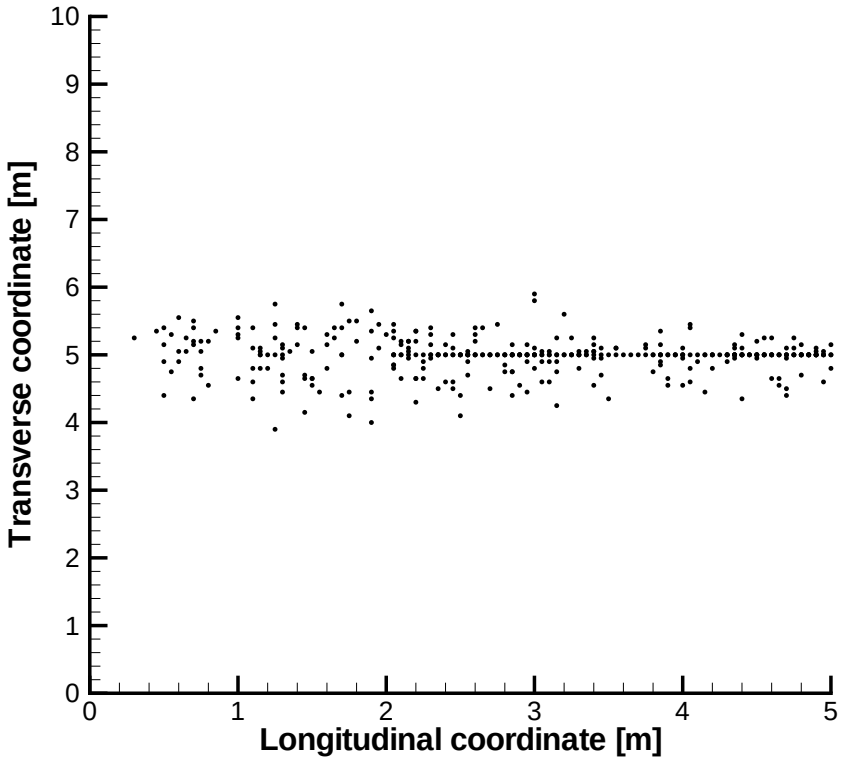

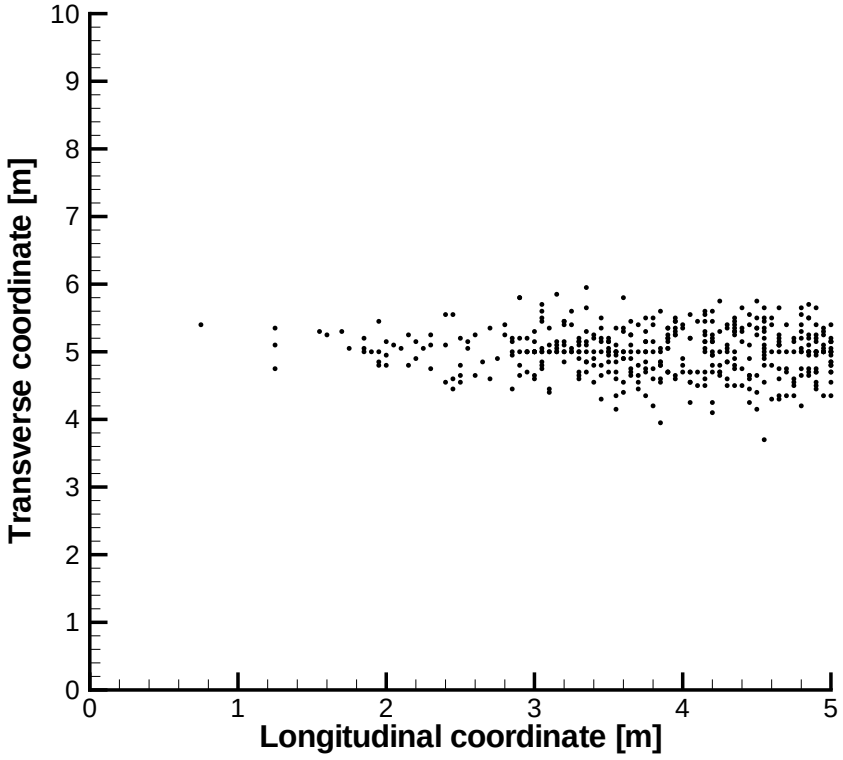

Figure 4-14. *Transients. Particle distribution at time* $3\times10^5 s$*, for* $f = 0.01$ *(top) and* $f = 0.1.v_{\max} = 0.1u$.

5 Discussion

When evaluating the simulations and models presented, one should first note that the problem addressed is not well defined. The goal is to predict the transport and retention processes, as manifested in the BTC. This for a range of tracers, with varying properties, and ultimately for any kind of rock fracture. The problem is not well defined because:

- Geometry. Information about gouge material, parallel flow channels, crossing fractures, etc is incomplete.
- Tracer properties. Estimates of sorption and diffusion coefficients are uncertain, especially so for in situ conditions.
- Retention processes. A long list of possible retention processes can be compiled. It is not clear when and where a certain process needs to be considered.

Partly for this reason a fairly general diffusion based simulation model has been formulated. In order to help the reader to formulate an opinion about this model, the strong and weak points (as seen by the authors) of the model will be listed.

Strong points

- Fracture specification. This aspect is due to the general features of DarcyTools. As briefly demonstrated in Task 6B2, it is possible to base a simulation on a detailed description of the fracture properties (porosity, FWS, conductivity, etc). Multiple pathways is accounted for by the fracture network and property variations within the fracture zones.
- Multirate diffusion model. It is an advantage to be able to consider "diffusion volumes" with a wide range of capacities and exchange rates. For the present task we can hence use the same specification of immobile zones for the 1D experimental time cases, as for the 3D natural condition cases.
- Numerically efficient. For all simulations presented 10^5 particles were used in the simulations. Recent developments of the algorithms made this possible.

Weak points

- Can not take detailed information about mineralogy and matrix properties into account, when available.
- For strongly sorbing tracers, it is possible that chemical reactions are more important than diffusive exchange. As our model is focused on diffusion, it may not be easy to accommodate these reactions.

6 Conclusions

A first attempt to simulate tracer transport and dispersion, using the computer code DarcyTools, is reported.

The simulations requested in Task 6A, 6B and 6B2 have been carried out. Verification and validation studies indicate that the simulation model gives plausible results for weakly and non sorbing tracers. For strongly sorbing tracers the results are more uncertain.

The role of near stagnant water in the fracture plane and the possible effects of transients are discussed. A simple generic test case shows that transient pulses may displace a tracer and hence affect the breakthrough curve.

7 References

Barten, W. 1996. Linear response concept combining advection and limited rock matrix diffusion in a fracture network transport model. Water Resources Research, Vol. 32, No. 11, Pages 3285-3296.

Benabderrahmane, Dershowitz, Selroos, Uchida, Winberg. 2000. Task 6. Performance assessment modelling using site charcterisation data, (PASC). SKB note.

Bossart, P., Hermanson, J. and Mazurek, M. 2001: Analysis of fracture networks based on the integration of structural and hydrogeological observations on different scales. Swedish Nuclear Fuel and Waste Management Company (SKB), Technical Report TR-01-21.

Cvetkovic, V., Selroos, J.O., Cheng, H. 1999. Transport of reactive tracers in rock fractures. J. Fluid Mech. Vol. 378, pp. 335-356.

Dershowitz, W., Cladouhos, T., Uchida M. 2000. Tracer tests with sorbing tracers. Äspö Task Force, Task 4E and 4F. SKB, ICR-01-02.

Dershowitz, W., Winberg, A., Hermansson, J., Byegård, J., Tullborg, E-L., Andersson, P., Mazurek, M. 2003. Äspö Task Force, Task 6c. Construction of a block scale semisynthetic hydrostructural models and attribution of hydraulic and transport properties. SKB IPR-03-13.

Elert, M., Svensson, H. 1999. Äspö Hard Rock Laboratory. Deconvolution of breakthrough curves from TRUE-1 tracer tests (STT-1 and STT-1b) with sorbing tracers. Äspö Task Force, Task 4E. SKB, IPR-99-35.

Elert, M., Svensson, H. 2001. Evaluating of modelling of the TRUE-1 radially converging tests with sorbing tracers, The Äspö Task Force on Modelling of Groundwater Flow and Transport of Solutes, Tasks 4E and 4F. SKB TR-01-12.

Haggerty, R., Gorelick, S. M. 1995. Multiple-rate mass transfer for modelling diffusion and surface reactions in media with pore-scale heterogeneity. Water Resources Research, Vol. 31, No. 10, Pages 2383-2400.

Haggerty, R., McKenna, S.A., Meigs L.C. 2000. On the late-time behavior of tracer test breakthrough curves. Water Resources Research, Vol. 36, No. 12, Pages 3467-3479.

Hakami, E. 1995. Aperture distribution of rock fractures. PhD-thesis TRITA-AMI PHD 1003. Royal Institute of Technology (KTH), Stockholm, Sweden.

Jacob, A., Mazurek, M. and W. Heer 2003. Solute transport in crystalline rocks at Äspö – II: Blind predictions, inverse modelling and lessons learnt from test STT1. Journal of Contaminant Hydrology, Vol. 61, pp. 175-190.

Mazurek, M., Jakob, A. and Bossart P. 2003. Solute transport in crystalline rocks at Äspö – I: Geological basis and model calibration. Journal of Contaminant Hydrology, Vol. 61, pp. 157-174.

Neretnieks, I. 2002. A stochastic multi-channel model for solute transport - analysis of tracer tests in fractured rock. Journal of Contaminant Hydrology 55(3-4): 175-211.

Selroos, J-O., Elert, M. 2001. Task 6A & 6B Modeling task specification Version 1.0, 3 April 2001.

Svensson, U., Kuylenstierna, H-O., Ferry, M. 2004. DarcyTools –Concepts, method, equations and demo simulations. SKB R-04-19.

Winberg, A., Andersson, P., Hermansson, J., Byegård, J., Cvetkovic, V., Birgersson, L. 2000. Äspö Hard Rock Laboratory, Final report of first stage of tracer retention understanding experiments, Swedish Nuclear Fuel and Waste Management Co, TR-00-07.

Appendix A, verification studies

Introduction

The objective of this study is to compare the solutions given by DarcyTools with the analytical solutions for single rate diffusion. The multi-rate diffusion model in DarcyTools is hence "degenerated" to a single rate model; this is done by specifying the late time slope, *k*, to -3/2.

The situation studied is outlined in Figure A1. A channel with constant width and aperture is bounded by an infinite matrix. A Dirac pulse injection is prescribed and the BTC at the outlet is studied.

The analytical solution of the equation describing this case is given by, for example, Barten (1996), Cvetkovic et al. (1999) and Neretnieks (2002). It can be written as:

$$m = \Theta(t-\alpha)\frac{\gamma}{2\sqrt{\Pi}}(t-\alpha)^{-3/2}\exp\left(-\frac{\gamma^2}{4(t-\alpha)}\right) \qquad \text{(A1)}$$

where *m* is mass flux at the outlet, $\Theta(t)$ Heaviside step function and *t* time. The two parameters α and γ are defined as:

$$\alpha = R_m\theta_m L/q, \qquad \text{(A2)}$$

$$\gamma = L\delta_f\theta_{im}\sqrt{D_w R_{im}}/q \qquad \text{(A3)}$$

with definitions of parameters as given in Table A1, below.

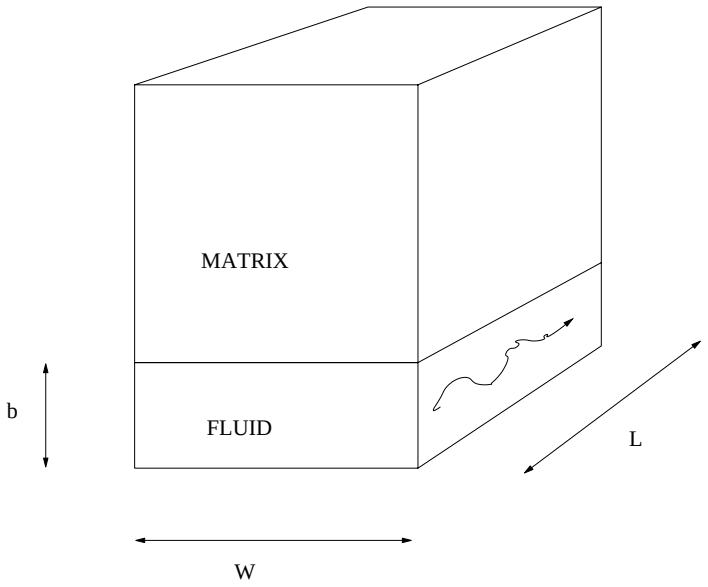

Figure A1. *Outline of situation studied.*

Numerical simulations

A reference case is given by the values specified in Table A1. The two parameters $\alpha_{\min}$ and $\alpha_{\max}$ are chosen to give a large enough range of capacity boxes. The specification of these does however influence the setting of β_n, the volume ratio for a non sorbing tracer. The analytical solution is for an infinite matrix, while a specification of $\alpha_{\min}$ implies a limitation. For this case a formula for β_n can be derived (unpublished note) that gives a $\beta_n = 20.85$.

Table A1. Simulation parameters.

Domain	$L = 10.0,\ W = 0.1,\ b = 0.5\times10^{-3}$ [m] Surface to volume ratio: $\delta_f = 1/b$ [m^{-1}]
Properties	Porosity mobile zone: $\theta_m = 1.0$ Porosity immobile zone: $\theta_{im} = 0.05$ Retention mobile zone: $R_m = 1.0$ Retention immobile zone: $R_{im} = 1.0$ Diffusivity: $D_w = 10^{-10}$ [m^2/s]
Transport	Flow velocity: $q = 10^{-5}$ [m/s] Injection: Dirac pulse $\alpha_{\min} = 10^{-9}/R_{im}$ [s^{-1}] $\alpha_{\max} = 5\times10^{-2}/R_{im}$ [s^{-1}]

Results/Discussion

First the volume ratio, β_n, was tested through the reference case. A value of 20.85 gives a perfect agreement with the analytical solution, see Figure A2. For the cases to follow β was evaluated as: $\beta = \dfrac{R_{im}V_{im}}{R_mV_m} = \dfrac{R_{im}}{R_m}\times\beta_n$.

In Figure A3 the effect of changing R_m and R_{im} by a factor of five can be studied. The change from the reference case is calculated correctly.

Figure A4 shows consistency checks, which are based on the parameters α and γ, given by (A2) and (A3) respectively. In the first case (Figure A4, top), R_m, q and θ_{im} were all increased by a factor of 2.0. As both α and γ remain the same, the BTC should be unaffected. This is also found. Similarly we may increase θ_{im} with a factor of two and decrease D_w with a factor of four and still get the same BTC, which is also the case (Figure A4, bottom).

Conclusion

It is clear that the numerical solutions, based on a particle tracking technique, is in good agreement with the analytical solution of the governing advection/diffusion equation.

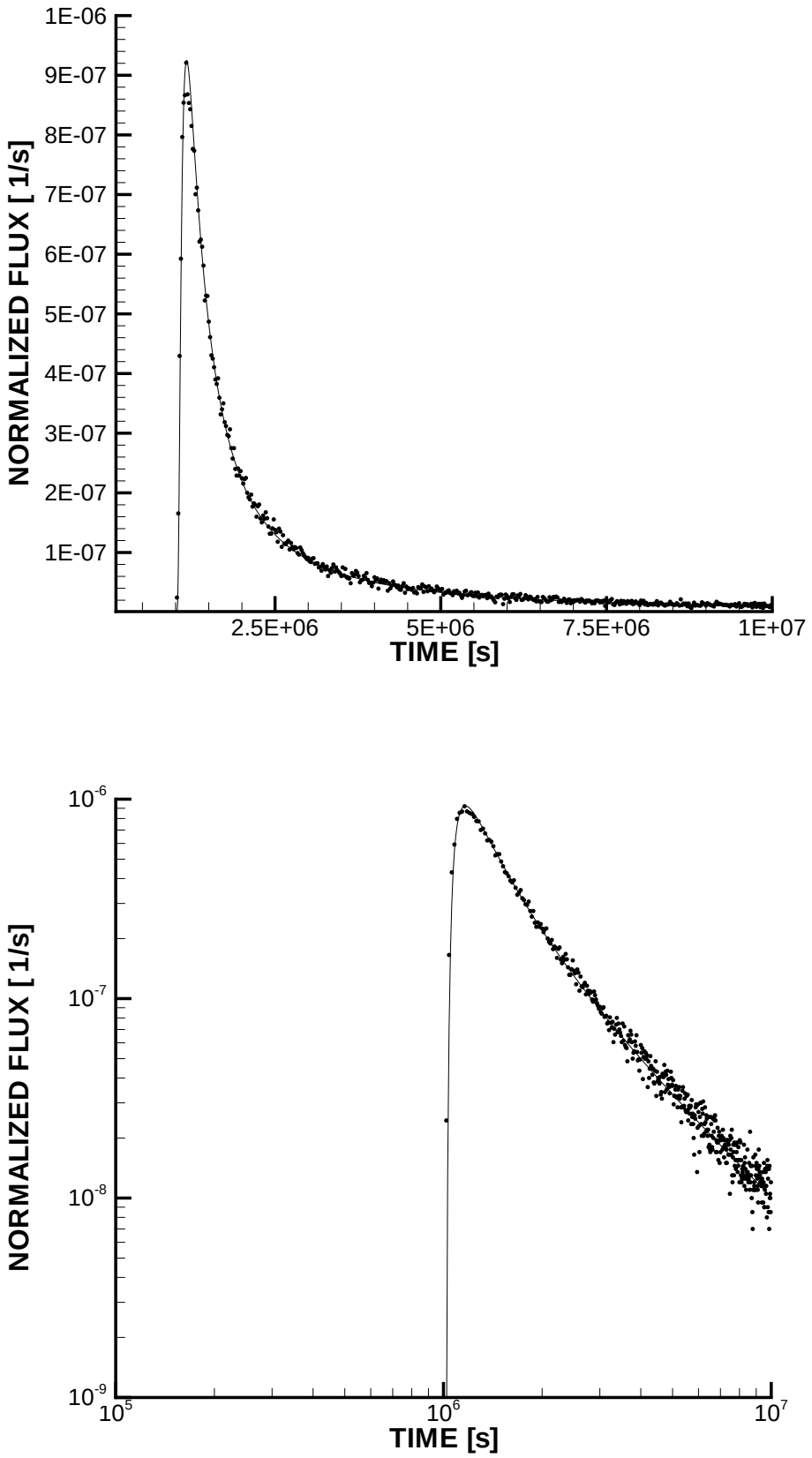

Figure A2. *Comparison with the analytical solution for the reference parameters. Linear scale (top) and log-log scale. Solid line gives analytical solution.*

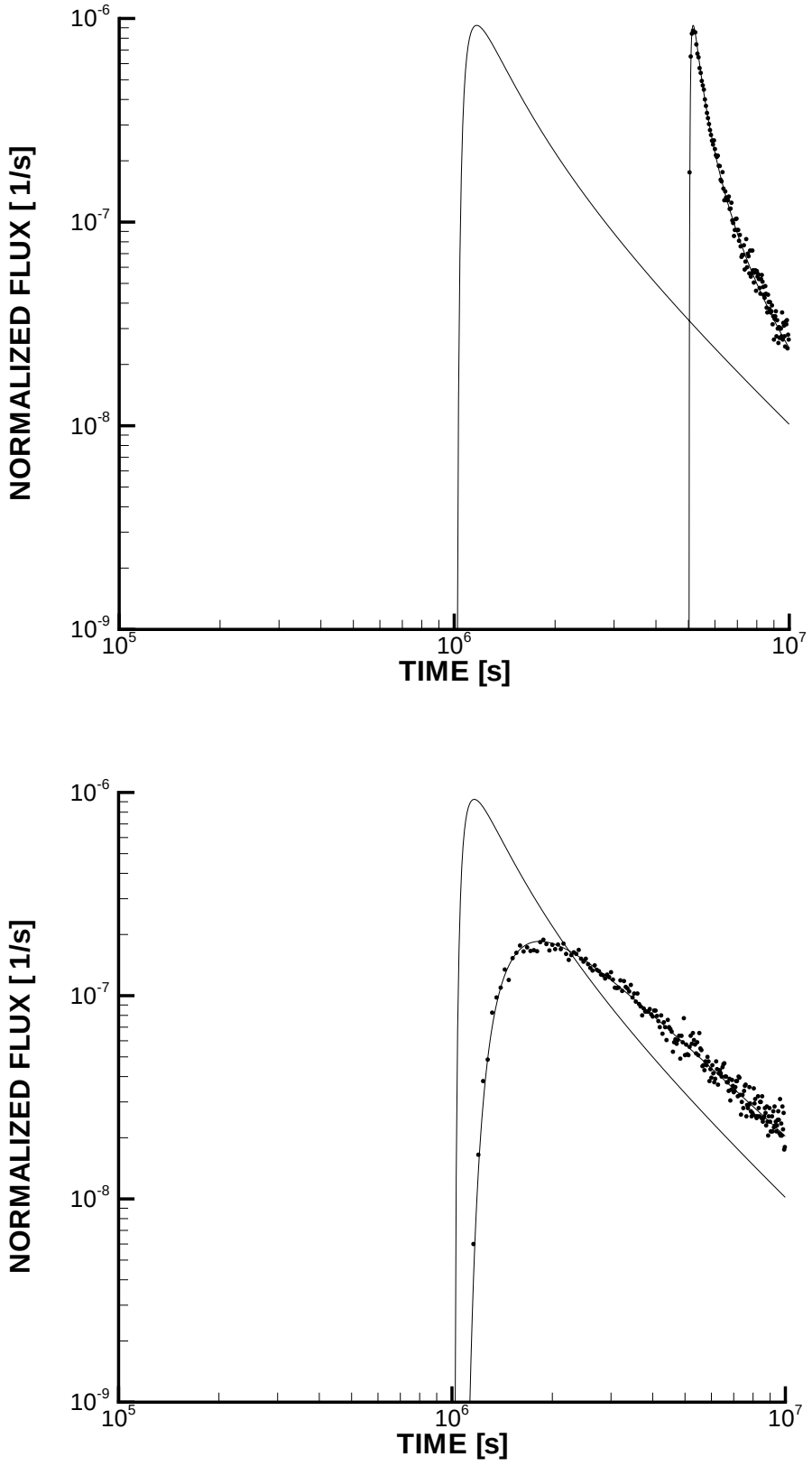

Figure A3. *Effect of changing R_m (top) and R_{im} by a factor of five. Solid line gives analytical solution.*

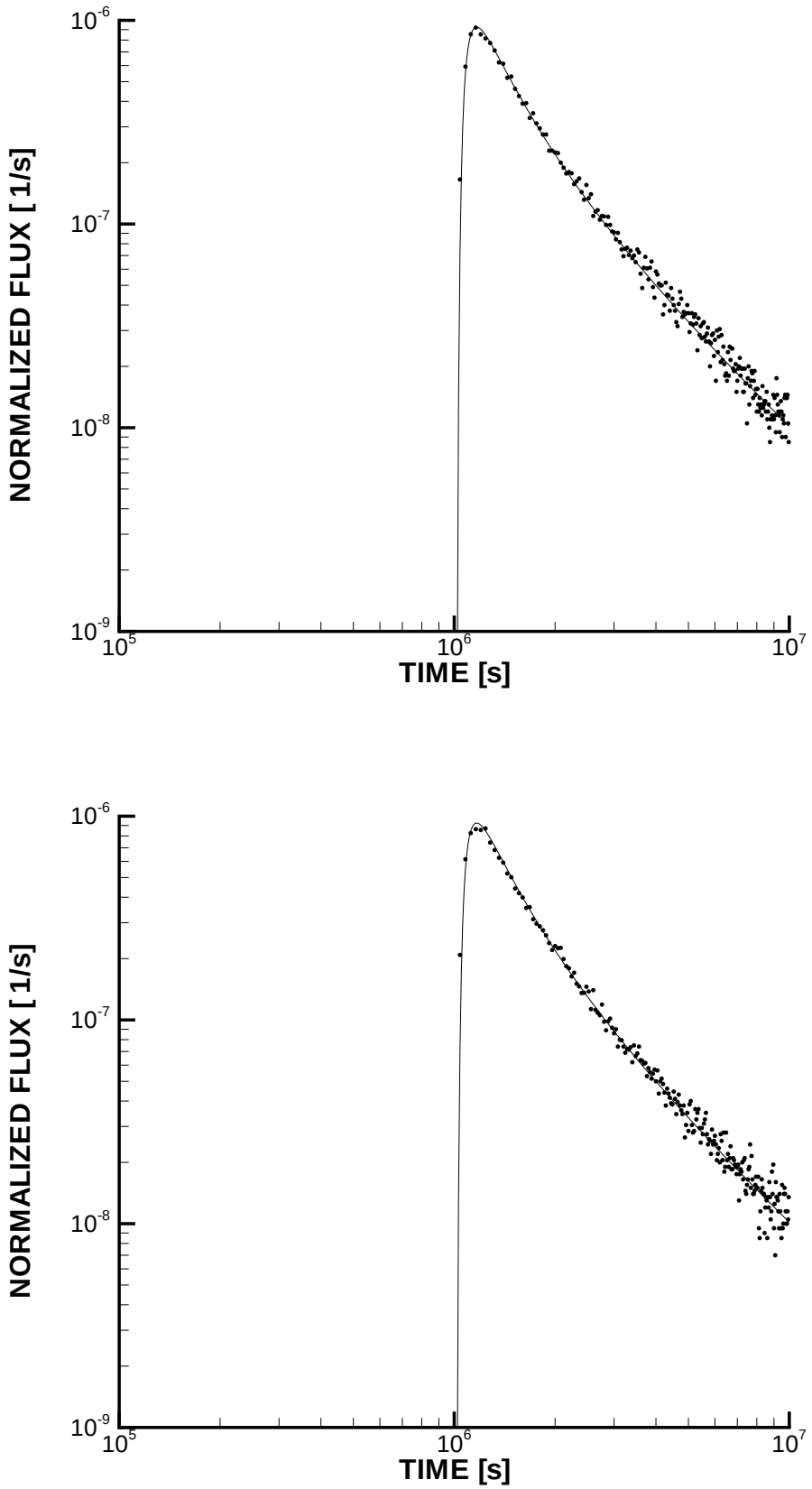

Figure A4. *Consistency checks.* R_m, q *and* θ_{im} *increased (top),* θ_{im} *increased and* D_w *decreased, (bottom). Solid line gives analytical solution.*

Appendix B, sensitivity studies

Introduction

It is useful to know how the model parameters affect the BTC in a typical simulation. It is the objective of this appendix to provide some information of that kind.

The situation studied is similar to the one outlined in Figure A1; some parameters of the reference case are however different (details below).

Numerical simulations

A set of parameters with numerical values are given in Table B1; these parameters define the reference case. Five variables: $l_{\min}$, R_m, R_{im}, β_n and k will be in focus in the sensitivity analysis. Note that some of the parameters are linked. As an example, changing R_{im} implies changes in β, $\alpha_{\min}$ and $\alpha_{\max}$.

Table B1. Simulation parameters.

Domain	$L = 5.0, W = 0.05, b = 0.5\times10^{-3}$ [m]
Properties	Retention mobile zone: $R_m = 1.0$ Retention immobile zone: $R_{im} = 1.0$ Diffusivity: $D_w = 10^{-9}$ [m^2/s] Smallest box: $l_{\min} = 10^{-3}$ [m]
Transport	Flow velocity: $q = 10^{-4}$ [m/s] Late time slope: $k = 1.75$ $\alpha_{\min} = D_w / \left(l_{\min}^2 \times R_{\min}\right)$ [s^{-1}] $\alpha_{\max} = 10^{-10} / R_{im}$ [s^{-1}] non-sorbing β: $\beta_n = 50$ Injection: Dirac pulse

Results/Discussion

The first parameter to be discussed is $l_{\min}$, see Figure B1. By choosing a smaller $l_{\min}$ we increase the capacity of fast boxes and the BTC will be somewhat delayed. Note that the peak value is not affected.

Next we study the effects of R_m and R_{im}, see Figure B2. R_m simply delays the transport in the mobile zone and the implications for the BTC are easy to understand. Note that the changing shape of the BTC is due to the logarithmic scale. Increasing R_{im} means that the total capacity of the immobile zone increases. The general effect of this is a delay and decrease of the peak.

Finally β and k are varied, see Figure B3. Increasing β means (similar to R_{im}) that the total capacity of the immobile zone increases. The late time slope value, k, determines how the capacities are distributed along the α-values. Increasing k means that capacity is moved to faster boxes and this will delay the transport in this case. This tendency may not be general, but for the present case the slowest boxes are probably inactive and by increasing k more capacity becomes involved in the retention process.

Conclusion

All results presented can be understood by physical reasoning. It is further of value to have the quantitative effects of the model parameters documented when validation studies are attempted (Appendix C).

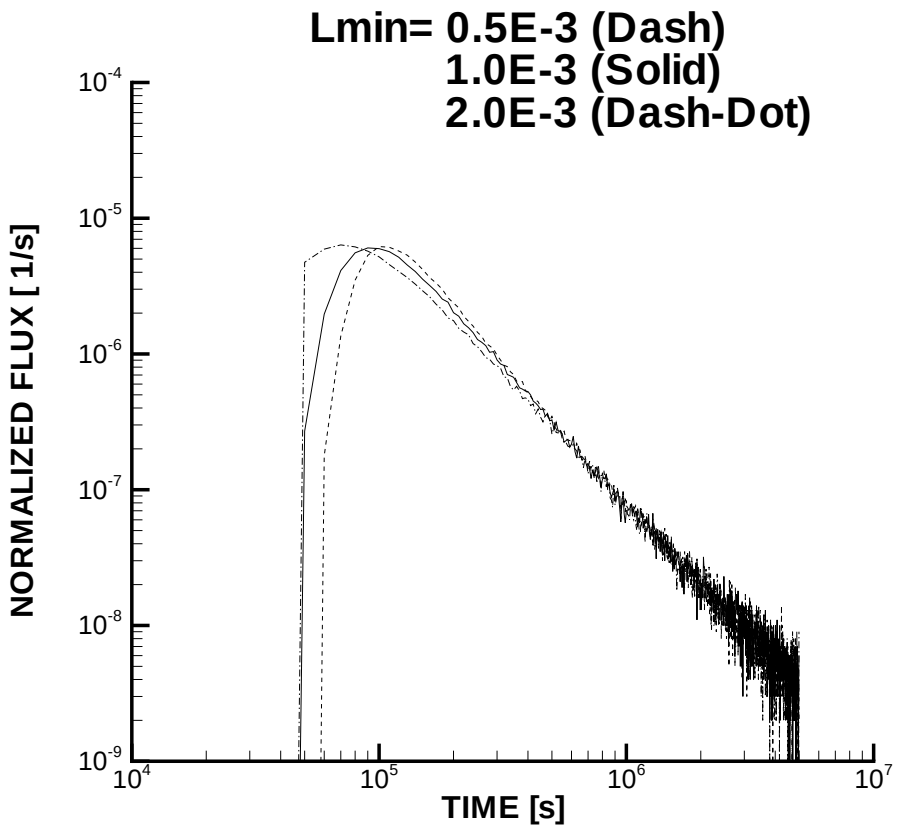

Figure B1. *Sensitivity studies. Effect of changing* $l_{\min}$.

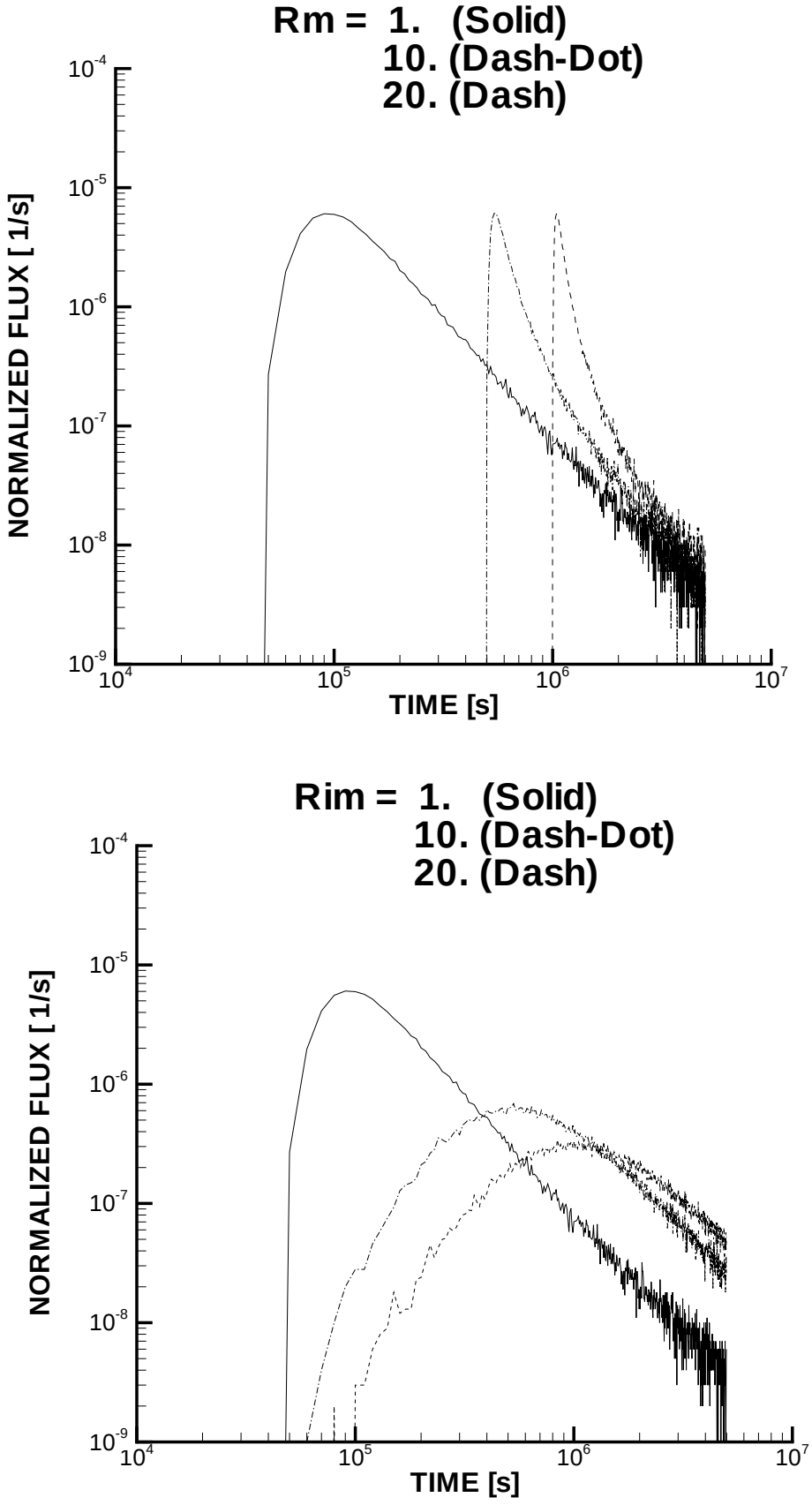

Figure B2. *Sensitivity studies. Effect of increasing* R_m *(top) and* R_{im}.

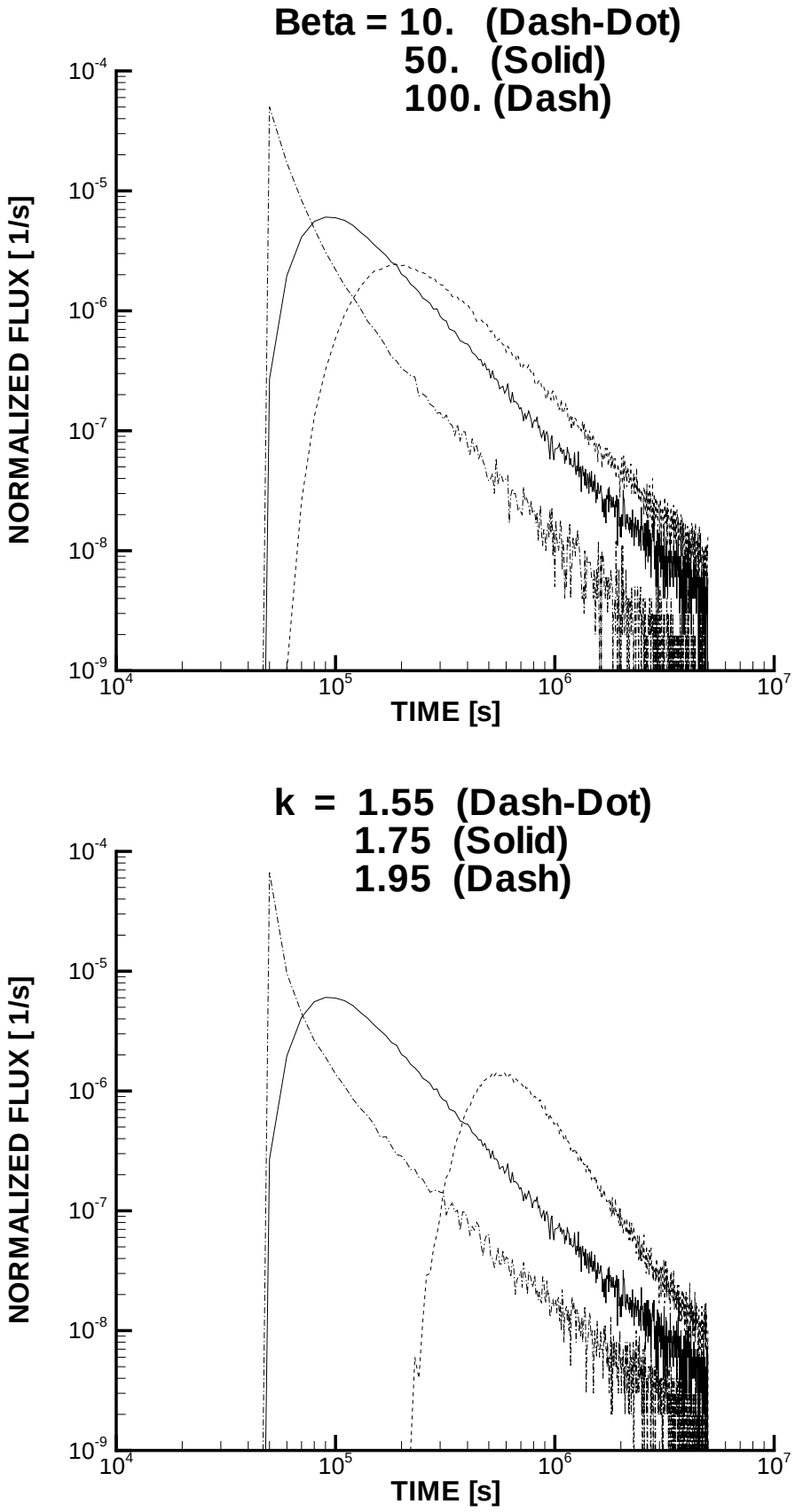

Figure B3. *Sensitivity studies. Effect of changing* β *(top) and k..*

Appendix C, validation studies

Introduction

Validation implies that the simulations should be compared with measurements. However, in this study a "somewhat derived form" of the field data will be used. The BTC:s measured in field have been deconvoluted to a unit response function, i.e. the BTC represents the expected result from a Dirac pulse input (see Elert and Svensson, 1999). For the present purpose we will however regard the deconvoluted BTC as field data.

The objective of the validation study is to show that the numerical model can be tuned to fit the experimental BTC:s. It is however not meaningful to use all model parameters in such a tuning or to use unrealistic values on parameters. A strategy is needed.

As this is the first comparison with field data, it is relevant to begin with a study that focuses on the most uncertain model parameters. We will call this study phase I. The real test of a tracer transport model is however to predict BTC:s. To do predictions, the model parameters should be known or possible to estimate without reference to the measured BTC. In phase II we will use fixed model parameters and only vary property data.

The problem specification is in most respects identical to the one given for Task 6A (see main report). Deviations from this specification will be listed and discussed.

Validation, phase I

If fracture and matrix properties, flow velocity, tracer properties, etc were all known the present model would still have two parameters that are undetermined:

- k, the late time slope. For a single rate diffusion problem we know that $k = 1.5$, but for more complex situations we can only say that $k > 1.5$. Haggerty et al. (2000) found, using a multi-rate model, that $k = 2.1 \rightarrow 2.2$ fits experimental data.
- $\alpha_{\max}$ (rate for the smallest boxes) is uncertain because it is not clear if we should associate the fastest boxes with diffusion into stagnant water or diffusive exchange with the matrix. In the later case $\alpha_{\max}$ should be estimated as $D_w / \left(l_{\min}^2 R_{im} \right)$ while one may question if R_{im} should be involved (fully or not at all) for the stagnant water interpretation.

In phase I, k and $\alpha_{\max}$ will hence be used as tuning knobs, with the objective to learn about sensitivity and limits. Some more conditions for the simulations:

- β_n (for non sorbing tracers) is first estimated. For sorbing tracers $\beta = R_{im} \times \beta_n / R_m$. R_{im} and R_m are estimated from the tracer data (see Table C-1).
- $\alpha_{\min} = 10^{-10}$ for HTO and $D_w / D_{w,HTO} \times 10^{-10} / R_{im}$ for other tracers.
- The unit response BTC:s include the following tracers: HTO, Uranine, Na22, Sr85, Rb86 and Co58 (see table C1).

Table C1. Tracer property data

Tracer	D_w $(\times 10^{-9})$ [m^2/s]	K_a [m]	K_d [m^3/kg]	R_m	R_{im}
HTO/Uranine	2.4	0.	0.	1.	1.
Na22	1.33	7×10^{-7}	1.4×10^{-6}	1.0	1.95
Sr85	0.78	8×10^{-6}	4.7×10^{-6}	1.02	4.2
Rb86	2.0	5×10^{-4}	4×10^{-4}	2.0	271.
Co58	0.5	8×10^{-3}	8×10^{-4}	17.	542.

The first BTC discussed is for HTO, see Figure C1. As data are available also for Uranine (which should give a similar BTC) we include the data for Uranine as well. It is found that $\beta_n = 4$ and $k = 2.2$ give an excellent agreement with the measurements. Note that $\alpha_{\max}$ is not uncertain for this case.

Next Na22 is considered. It is found from the measurements that "the peak is as high as for a non sorbing tracer, but delayed". It is not possible to obtain this effect, by the present model, without a $R_m > 1.0$. So, even if we set out to use the estimated values for R_m and R_{im}, we change R_m from 1.0 to 2.7, to get the peak arrival time right. $\alpha_{\max}$ is estimated to be in the range $0.68 \rightarrow 1.33\times10^{-3}$. A $k = 2.05$ and $\alpha_{\max} = 0.68\times10^{-3}$ give a fair agreement with measurements, as seen in

Figure C2.

Strontium is the next, weakly sorbing, tracer to be studied. $\alpha_{\max}$ should be in the interval $0.19 \rightarrow 0.78\times10^{-3}$. A somewhat larger value, 1.3×10^{-3}, and a $k = 2.05$ are needed to ensure good agreement, see Figure C3.

For Rubidium the $\alpha_{\max}$ interval is $0.74\times10^{-5} \rightarrow 2.0\times10^{-3}$. A $\alpha_{\max} = 1.1\times10^{-4}$ and a $k = 1.86$ give a fair agreement, see Figure C4, with the measured BTC.

Cobalt is the final tracer to be discussed. The $\alpha_{\max}$ interval is now $0.92\times10^{-6} \rightarrow 0.5\times10^{-3}$. A $k = 2.0$ and $\alpha_{\max} = 1.5\times10^{-5}$ is the best two-parameter tuning that could be found. The agreement with the measured BTC, see Figure C5, is however not very good.

Validation, phase II

The objective is now to evaluate how well we can tune the model to the experimental data by only changing tracer property data, as represented by R_m and R_{im}. We then need to conclude something about *k* and $\alpha_{\max}$ from phase I. The *k* values range from $1.86 \rightarrow 2.2$. Let us put $k = 2.0$. $\alpha_{\max}$ was found to be in the expected range, except for Sr85. It is however difficult to make further interpretations of the comparisons. In lack of further evidence, $\alpha_{\max}$ will be based on the $\log_{10}$ average of the two limits (i.e. the average of 10^{-5} and 10^{-3} is 10^{-4}).

Again we start with HTO and estimate β_n. Now we only have one parameter to tune as HTO is non sorbing. A $\beta_n = 10.0$ gives a fair agreement as can be seen in Figure C6. One should however note that $k = 2.0$ is not the best value for the part after the peak (compare with Figure C1).

For Na22, see Figure C7, $R_m = 2.0$ and $R_{im} = 1.0$ give a good agreement, with the same arguments as in phase I. The estimated values, see Table C1, are $R_m = 1.0$ and $R_{im} = 1.95$.

For SR85 $R_m = 2.5$ and $R_{im} = 2.0$ produce a fair agreement, see Figure C8. These values are of the same magnitude as estimated.

In Figure C9, the comparison for Rubidium is shown. $R_m = 2.0$ and $R_{im} = 30.0$ were used in the simulation ($R_m = 2.0$ and $R_{im} = 271$ in Table C1). However, the "average rule" for $\alpha_{\max}$ did not produce a good agreement for the early part of the BTC. A reduction, from $0.37 \rightarrow 0.07 \times 10^{-3}$, gives a significant improvement. Both curves are shown in Figure C9.

The same holds true for Cobalt, see Figure C10. The $\alpha_{\max}$ based on the average is 2.1×10^{-5}, while the better BTC is based on $\alpha_{\max} = 0.5 \times 10^{-5}$. For both curves the estimated $R_m (= 17)$ and $R_{im} (= 542)$ were used.

Concluding remarks

In the discussion section of the main report some comments about the advantages and limitations of the present model can be found. These comments are to a large extent based on the simulations presented in this Appendix.

It is difficult to establish the "predictive capability" of the model from the simulations presented. What can be said is that using: $\beta_n = 10$, $k = 2.0$, the averaging law for $\alpha_{\max}$ and the estimated values for R_m and R_{im}, we can optain BTC:s that are in fair agreement with measured data for non-sorbing to weakly sorbing tracers. No claims can be done for strongly sorbing tracers.

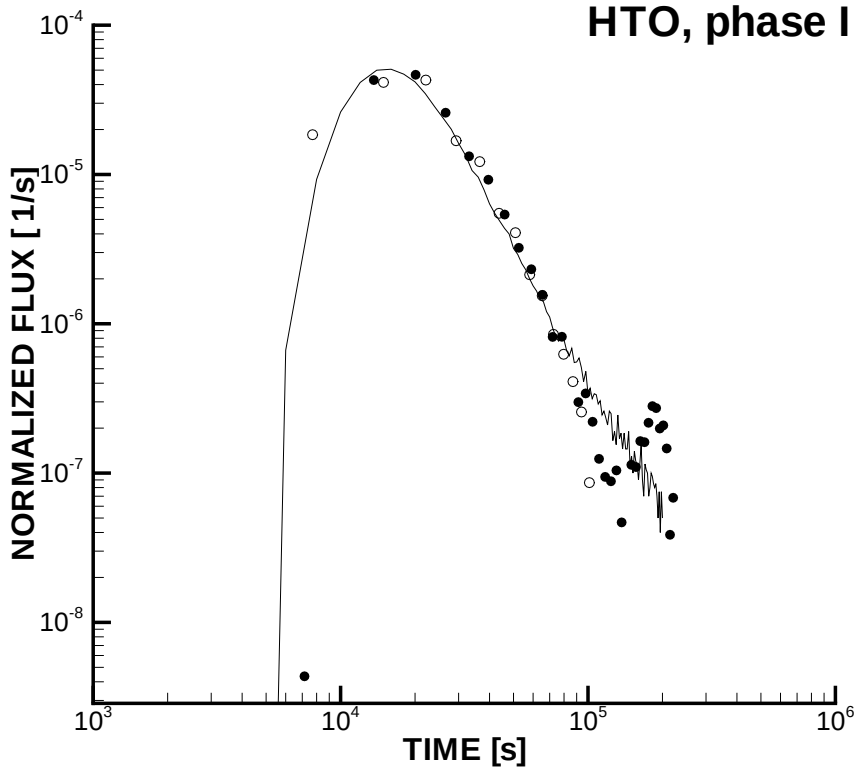

Figure C1. *Validation, phase I. Solid line gives simulation, circles measurements. Open circles HTO and filled circles Uranine.*

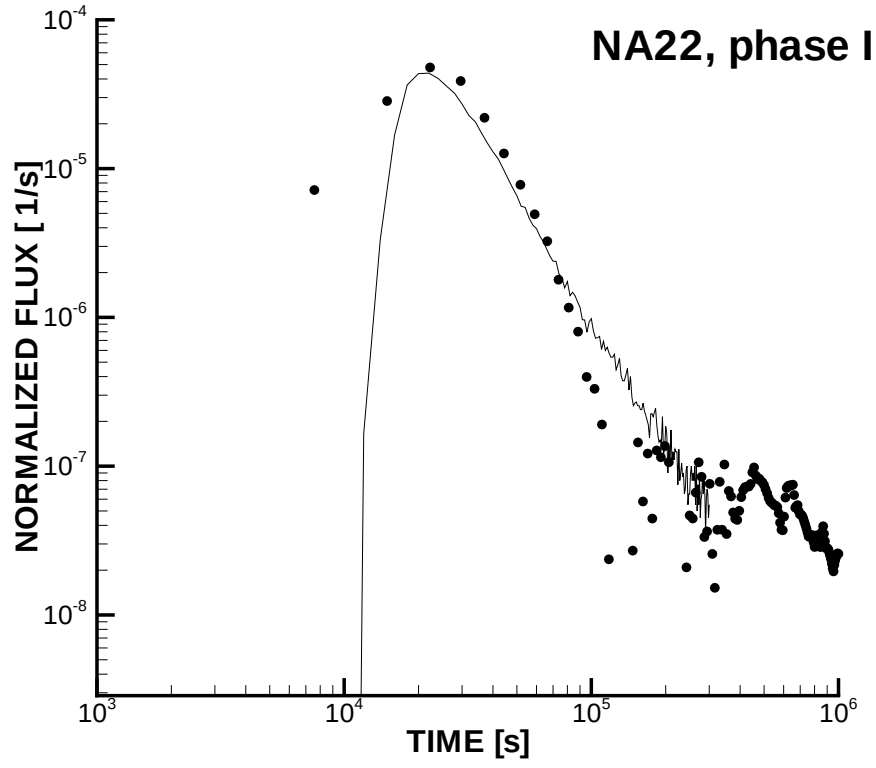

Figure C2. *Validation, phase I. Solid line gives simulation, circles measurements.*

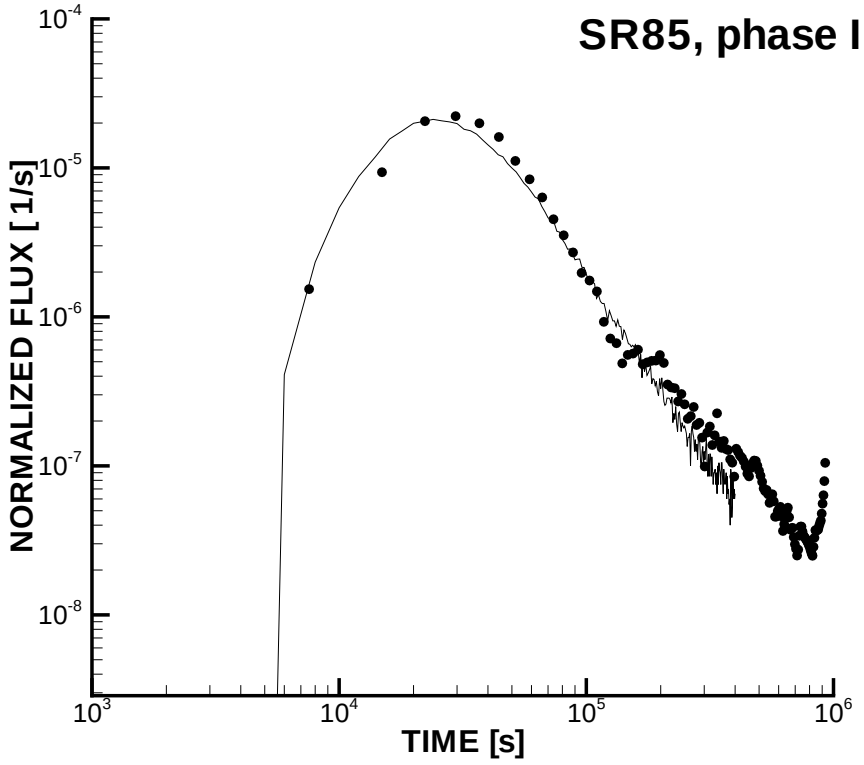

Figure C3 *Validation, phase I. Solid line gives simulation, circles measurements.*

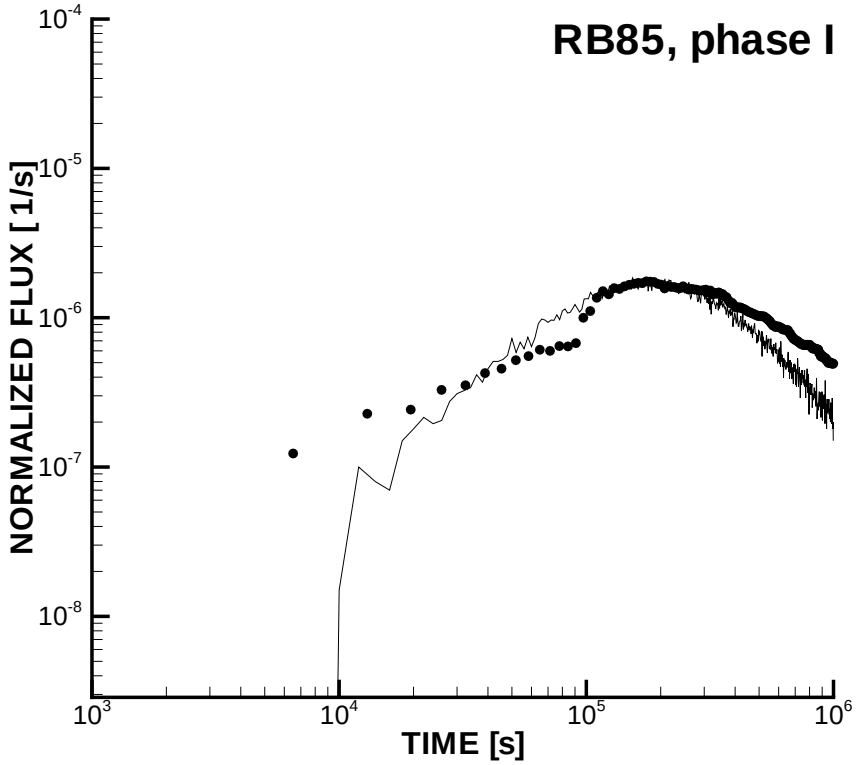

Figure C4. *Validation, phase I. Solid line gives simulation, circles measurements.*

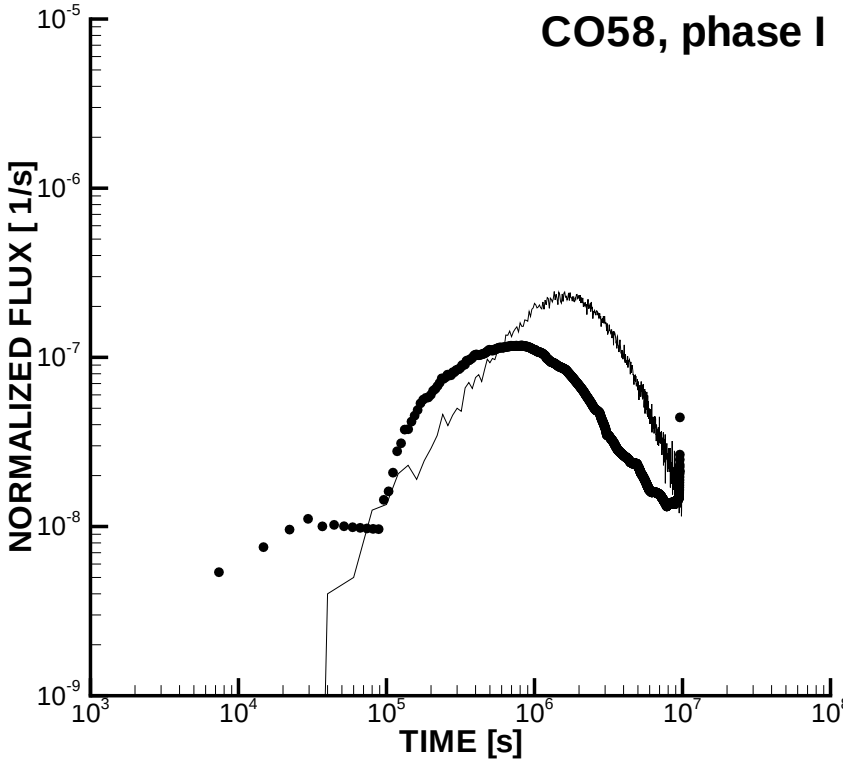

Figure C5. *Validation, phase I. Solid line gives simulation, circles measurements.*

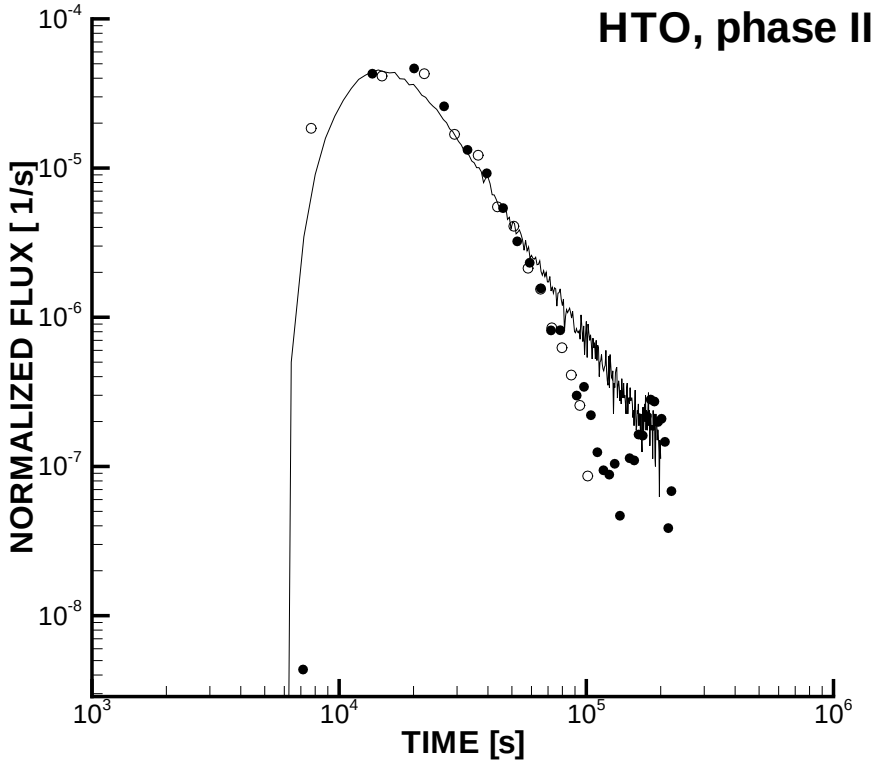

Figure C6. *Validation, phase II. Solid line gives simulation, circles measurements. Open circles HTO and filled circles Uranine.*

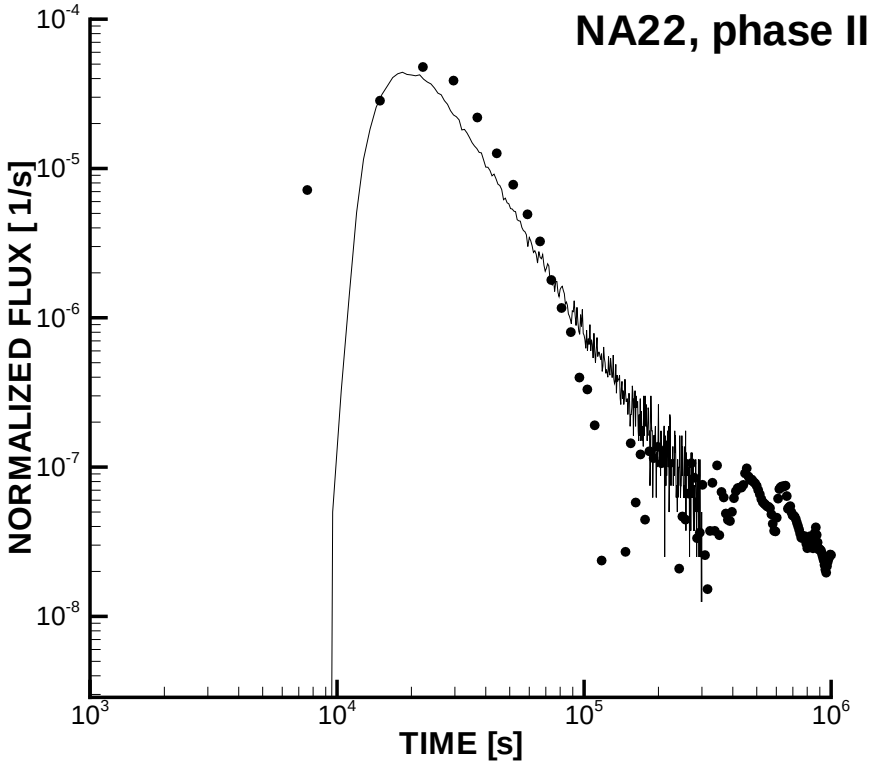

Figure C7. *Validation, phase II. Solid line gives simulation, circles measurements.*

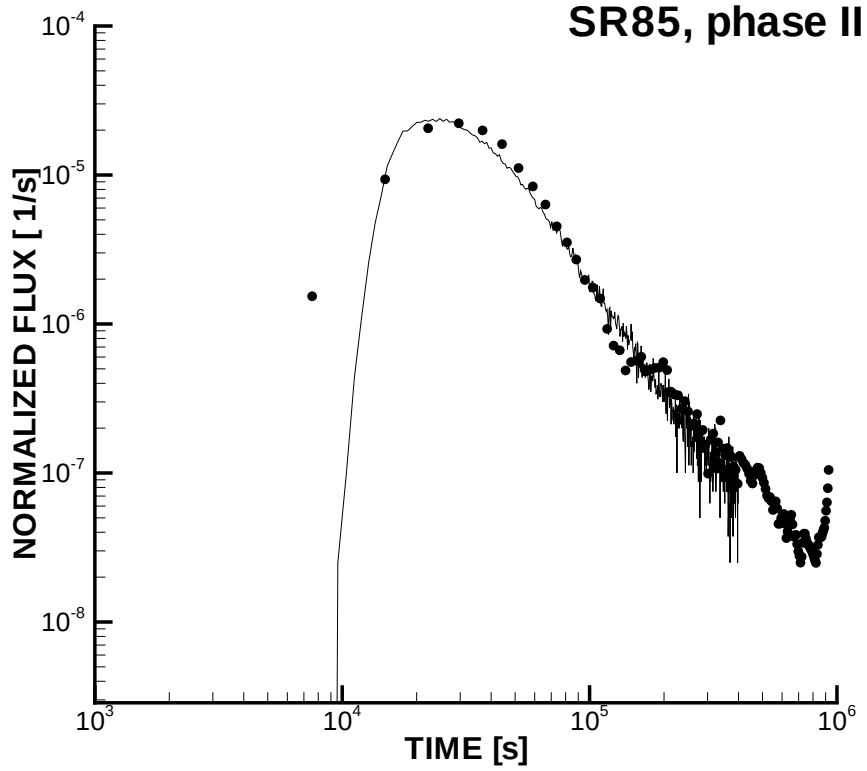

Figure C8. *Validation, phase II. Solid line gives simulation, circles measurements.*

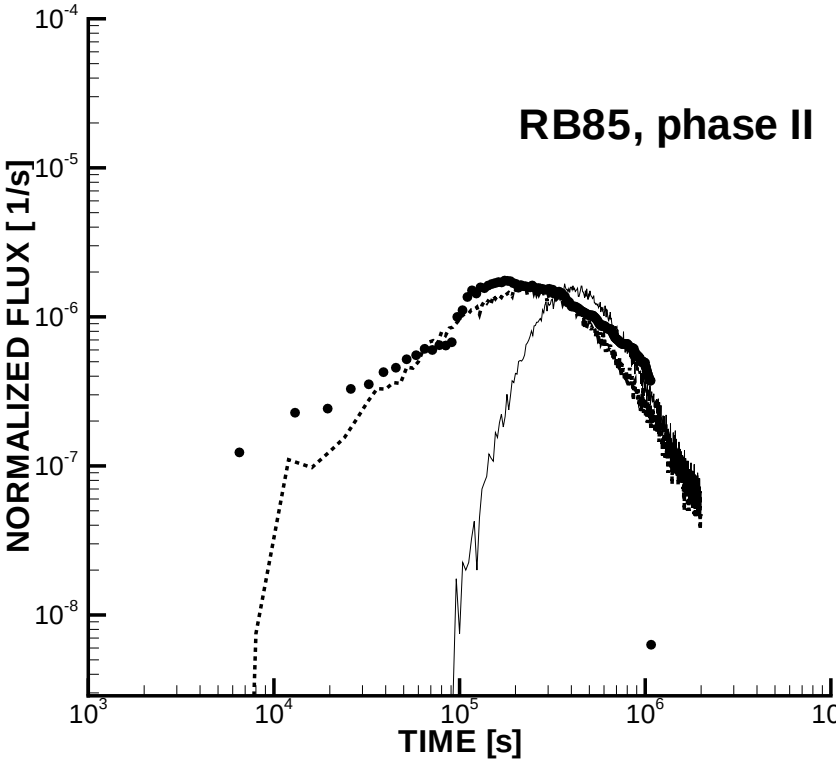

Figure C9. *Validation, phase II. Solid line gives simulation, circles measurements.. Dashed line gives simulation with reduced* $\alpha_{\max}$.

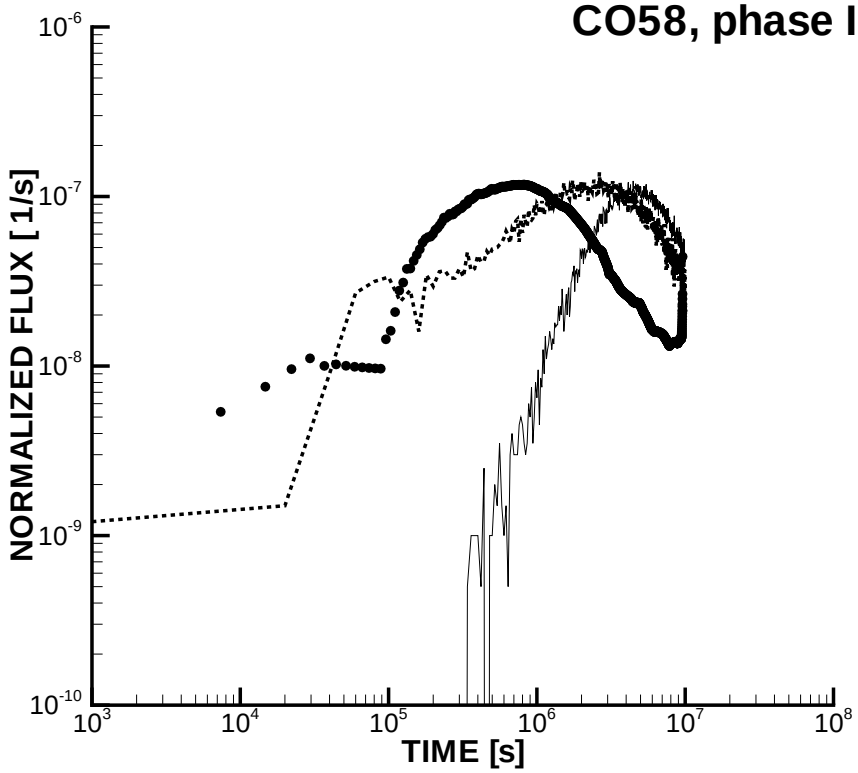

Figure C10. *Validation, phase II. Solid line gives simulation, circles measurements. Dashed line gives simulation with reduced* $\alpha_{\max}$.